The impact of resolving sub-kilometer processes on aerosol-cloud interactions in global model simulations

C. R. Terai [1,2], M. S. Pritchard [1], P. Blossey [3], and C. S. Bretherton [3]

[1]Department of Earth System Science, University of California, Irvine, CA, USA
[2]Lawrence Livermore National Laboratory, Livermore, CA, USA
[3]Department of Atmospheric Sciences, University of Washington, Seattle, WA, USA

Key Points:

- Aerosol-cloud interactions in a global model that resolves sub-kilometer processes are compared to those in a coarser 3km model.
- Resolving sub-kilometer scales leads to a weaker increase in liquid water path with aerosols.
- Weaker LWP increase is due to fewer precipitating clouds and weaker LWP increase in non-raining clouds.

Corresponding author: Christopher R Terai, crterai@gmail.com

Abstract

Sub-kilometer processes are critical to the physics of aerosol-cloud interaction but have been dependent on parameterizations in global model simulations. We thus report the strength of aerosol-cloud interaction in the Ultra-Parameterized Community Atmosphere Model (UPCAM), a multiscale climate model that uses coarse exterior resolution to embed explicit cloud resolving models with enough resolution (250-m horizontal, 20-m vertical) to quasi-resolve sub-kilometer eddies. To investigate the impact on aerosol-cloud interactions, UPCAMs simulations are compared to a coarser multi-scale model with 3 km horizontal resolution. UPCAM produces cloud droplet number concentrations (N_{d}) and cloud liquid water path (LWP) values that are higher than the coarser model but equally plausible compared to observations. Our analysis focuses on the Northern Hemisphere midlatitude oceans, where historical aerosol increases have been largest. We find similarities in the overall radiative forcing from aerosol-cloud interactions in the two models, but this belies fundamental underlying differences. The radiative forcing from increases in LWP is weaker in UPCAM, whereas the forcing from increases in N_{d} is larger. Surprisingly, the weaker LWP increase is not due to a weaker increase in LWP in raining clouds, but a combination of weaker increase in LWP in non-raining clouds and a smaller fraction of raining clouds in UPCAM. The implication is that as global modeling moves towards finer than storm-resolving grids, nuanced model validation of ACI statistics conditioned on the existence of precipitation and good observational constraints on the baseline probability of precipitation will become key for tighter constraints and better conceptual understanding.

Plain Language Summary

How aerosol particles impact the climate through their interactions with clouds is a significant source of uncertainty in quantifying the drivers of climate change over the past hundred years. Global climate models have so far been heavily reliant on approximations of the physical processes that occur at sub-kilometer scales, even though processes at those scales are important for representing the physics behind aerosol-cloud interactions. To address this gap, we develop and run a multi-scale global model that embeds a finer-scale model (250-m in the horizontal and 20-m in the vertical) within the columns of a coarser resolution global model. A pair of simulations with pre-industrial and present-day aerosol emissions are used to quantify the impact of human aerosol emissions. They show that the climate impact of resolving sub-kilometer resolutions is relatively small. However, this masks some key differences. The increase in cloud water with increasing aerosols is substantially weaker when sub-kilometer motions are resolved. Most of this weakening is due a weaker response in non-raining clouds and there being fewer clouds that rain in the high resolution model. The simulation results point to observations of specific processes that can help further constrain the impact of aerosols on clouds and climate.

1 Introduction

The cloud radiative response to anthropogenic aerosol emissions, commonly called aerosol-cloud interaction (ACI), is a key contributor to historical and future climate change and the largest uncertainty of all present-day anthropogenic-driven radiative forcings (IPCC, 2014)). Numerous cloud regimes and mechanisms contribute to this uncertainty. Process studies have shown various pathways by which aerosols can impact cloud radiative properties, especially those of low-level liquid cloud, which respond through direct perturbations to cloud droplet number (Twomey, 1977), through changes in cloud thickness, cloud cover, and cloud lifetime due to the suppression of precipitation (Albrecht, 1989; Pincus & Baker, 1994), and through entrainment feedbacks (Ackerman et al., 2004; Bretherton et al., 2007; Hill et al., 2009).

Representing many of the key ACI mechanisms highlighted above requires accounting for effects of the cloud-forming eddies ($\mathcal{O}$ 100 m) in the planetary boundary layer. Therefore, one of the biggest challenges in studying ACI in global model simulations has been the range of scales that need to be considered to provide global estimates of aerosol radiative forcing. Present-day state-of-the-art global climate models (GCMs) have horizontal resolutions of order 100 km, and that has necessitated the reliance on parameterizations to represent subgrid variability and processes, such as convection and turbulence. Advances in supercomputing now mean that global storm-resolving models can be run on uniform meshes with horizontal spatial resolutions of 0.8-3 km (Sato et al., 2018; Stevens et al., 2019). However, it will still be decades until we arrive at global simulations that resolve sub-kilometer resolutions (Schneider et al., 2017) that are necessary to begin resolving planetary boundary-layer eddies.

To fill this gap, global models built using a multi-scale modeling framework (MMF) allow strategic undersampling of horizontal space in order to better resolve subgrid scales by replacing parameterizations of subgrid motion and variability with explicit cloud resolving models (CRMs) embedded within GCM columns with typical spatial resolutions of >100 km (Grabowski, 2001; D. Randall et al., 2003; Khairoutdinov et al., 2005). In the past decade, despite their current limitations (e.g. idealized 2D turbulence that is locally periodic), MMFs have proved important for understanding some important effects of explicit deep convection on planetary scales (D. A. Randall, 2013). Today, MMFs likewise allow an advance look at the role of boundary-layer turbulence on global ACI. In the context of aerosol-cloud interactions, past studies using MMF with 4 km grid resolution that resolv deep cumulus updrafts but not boundary-layer eddies report that aerosol-cloud interactions are weaker in these multi-scale models than in conventionally-parameterized GCMs (Wang, Ghan, Ovchinnikov, et al., 2011; Kooperman et al., 2012).

In this study, we employ the Ultra-Parameterized Community Atmosphere Model, a version of MMF that has a drastically increased resolution of the embedded CRM. This allows the worlds first global climate model that also begins to resolve the outer scales of the boundary layer turbulent eddies that form low clouds. Early studies with UPCAM have shown that it has more realistic turbulence in cloud topped boundary layers than lower resolution MMFs and has high enough resolution at the top of boundary layer clouds to begin resolving the cloud-top entrainment processes (Parishani et al., 2017), which are important for key ACI processes like the sedimentation-entrainment feedback.

A secondary goal of the paper is to evolve best practices for diagnosing ACI physics underlying sensitivities in the era of increasingly explicit global simulations. Facilitating the comparison of global ACI simulations with high-resolution model simulations or with observations requires analyses beyond just examining the aggregated cloud radiative changes due to aerosol perturbations. On the one hand, analyses using process-oriented diagnostics highlight the importance of precipitation forming microphysical processes in the models (Wang et al., 2012; Suzuki et al., 2013; Michibata et al., 2016; Jing & Suzuki, 2018; Mlmenstdt et al., 2020). Progress has also been made in finding meteorological regimes in which GCMs respond similarly to aerosol perturbations (e.g., S. Zhang et al., 2016), but we still struggle to identify which processes cause the response of GCMs to diverge in other meteorological regimes. Because models differ in their parameterizations and in the way subgrid-scale cloud processes are represented, the difficulty of identifying the drivers of aerosol-cloud interactions in GCMs and observations is as much a conceptual problem as a technical one. Recent analyses (Chen et al., 2014; Toll et al., 2017) point to the distinction of raining and non-raining clouds in helping us better conceptually understand how clouds respond to aerosol perturbations and where areas of agreement and disagreement between models and observations lie. This study builds on such a framework to distinguish between the raining-cloud and non-raining cloud response in two separate models.

In Section 2, we first describe the prognostic aerosol version of UPCAM and the unique simulation strategy used to run ACI simulations given the considerable computational costs of the model. Then we show that — despite lack of model tuning — UPCAM is competitive with previous models in capturing cloud properties relevant for ACI (Section 3). We also demonstrate how a new analysis that utilizes the nudged-wind framework of previous studies allows us to test whether the mechanisms underlying our understanding of ACI are similarly simulated across different configurations of the same host model. And finally, we summarize our findings and highlight processes that need more observational constraints and further limited-area high-resolution simulations to hone in on key uncertainties in order to further constrain the strength of aerosol-cloud interactions (Section 4).

2 Methods

2.1 Ultra-Parameterized Community Atmosphere Model with prognostic aerosols

The goal of this study is to investigate the impact of resolving sub-kilometer eddies in a global simulation of aerosol-cloud interactions. For our modeling simulations we have expanded the capabilities of the Ultra-Parametrized Community Atmosphere Model (UPCAM) beyond what was introduced in Parishani et al. (2017) and Parishani et al. (2018) to incorporate prognostic aerosols and double moment microphysics in the cloud scheme.

UPCAM uses Version 5 of the Community Atmosphere Model (CAM5 – Neale et al., 2012) as its host GCM with a finite-volume dynamical core. For its physical parameterizations, CAM5 uses the microphysics scheme of Morrison and Gettelman (2008), the shallow cumulus scheme of Park and Bretherton (2009), the turbulence scheme of Bretherton and Park (2009), the deep convection scheme of G. J. Zhang and McFarlane (1995), and the RRTMG radiation scheme (Mlawer et al., 1997; Iacono et al., 2008). The model uses the 3-mode prognostic Modal Aerosol Model (MAM3 – Liu et al., 2012). In UPCAM, as in the Super-Parameterized Community Atmosphere Model (SPCAM – Khairoutdinov et al., 2005) from which UPCAM was developed, a smaller cloud-resolving model (CRM) is embedded in each column of CAM5 to represent the cloud-scale motions and processes that are typically represented by cloud and turbulence parameterizations in typical GCMs. UPCAM makes three notable changes to the SPCAM configurations that have previously been used to study aerosol-cloud interaction (Wang, Ghan, Easter, et al., 2011; Kooperman et al., 2012; K. Zhang et al., 2014). First, the horizontal grid spacing of the cloud resolving model (CRM) grid has been shrunk from approximately 4 km down to 250 m. Second, the vertical resolution has been increased from 30 levels to 120 levels, with most of the resolution increases concentrated in the lowest 3 km of the model, where the atmospheric boundary layer resides. Third, to offset the computational costs incurred by increasing the resolution of the cloud resolving model, the domain extent of the embedded cloud resolving model has been shrunk from typical extents of 128-256km down to 8 km. More details on UPCAM can be found in Parishani et al. (2017).

To enable the study of aerosol-cloud interactions, we have combined the existing UPCAM framework (Parishani et al., 2017) with the explicit-cloud parameterized pollutant scheme (ECPP), which uses statistics from the cloud resolving model to parameterize aerosol transport and wet scavenging (Gustafson et al., 2008; Wang, Ghan, Easter, et al., 2011). After reducing the internal timesteps within ECPP and the frequency with which we call ECPP, we have produced a model that produces large eddies in the boundary layer and prognoses the impact of those cloud updrafts on the activation of interactive aerosols. We compare the aerosol-cloud interaction in UPCAM with SPCAM and CAM5.

2.2 Simulation boundary conditions

All simulations use year 2000 climatological SST forcing, insolation, CO2 concentration, and stratospheric ozone concentrations. The pre-industrial simulation and the present-day simulation differ based on the aerosol and aerosol-precursor emissions, namely anthropogenic SO2, black carbon, and primary organic matter, created for the IPCC AR5 experiments and described by Liu et al. (2012) and (Wang, Ghan, Ovchinnikov, et al., 2011). The land model in all simulations is initialized by a January 1st land condition produced from a 25 year simulation with the baseline CAM5 model.

2.3 Computational constraints and simulation strategy

Despite the limited horizontal extent of the embedded CRMs, the addition of the prognostic aerosols and double moment microphysics increases the already high computational cost of these simulations. Even when run with a coarse $4^\circ \times 5^\circ$ (latitude $\times$ longitude) GCM, UPCAM completes 0.05 simulated years per day of computation when run on 828 cores.

To quantify aerosol-cloud interaction, we compare a simulation with present-day emissions and another simulation with the same boundary conditions, but with pre-industrial aerosol emissions. Due to meteorological differences that will arise between these two simulations, retrieving the aerosol signal from the internal variability typically requires multi-year simulations (Wang, Ghan, Ovchinnikov, et al., 2011; Kooperman et al., 2012), which are beyond our computational constraints. Previous studies by Kooperman et al. (2012) and K. Zhang et al. (2014) have shown the signal of the aerosol-cloud interactions can be retrieved from much shorter simulations, on the order of one year, if the meteorological variability is controlled by nudging the wind fields in the models to a common meteorological field using Newtonian relaxation. In this study, only the horizontal winds of the model are nudged to those of year 2008 in the European Centre for Medium-range Weather Forecasting Interim Reanalysis product (Dee et al., 2011). They are nudged every GCM timestep (5 min for UPCAM) to 6 hourly reanalysis fields with a relaxation timescale of also 6 hours.

Because a continuous 52-week simulation covering the whole year would still take a better part of a year to complete, we further reduce the amount of time it takes for us to arrive at the answer by running twelve separate six-week simulations starting at the beginning of each calendar month. As it takes roughly two weeks for the aerosol optical depth to reach roughly 80% of the global AOD values (liquid water paths equilibrate within a week), we remove the first two weeks of simulation and use the remaining four weeks of simulation for analysis. For consistency, we apply the same simulation strategy for both the CAM5 and SPCAM model simulations. We acknowledge that this simulation strategy may lead to slight underestimation of the aerosol concentrations in each simulation. We therefore choose a region of analysis that experiences the largest changes in directly emitted aerosol concentrations.

2.4 Observations

For observational comparisons with the present-day simulations, we use two satellite-based cloud retrieval: the liquid water path retrieval of Elsaesser et al. (2017) and the cloud top droplet number concentration retrieval of Grosvenor et al. (2018).

3 Results

3.1 Difference in present-day cloud properties across models

The droplet number concentration (N_{d}) at cloud top is a key indicator of aerosol-cloud interaction, and estimates of cloud-top N_d have been retrieved from satellite observations (e.g., Bennartz, 2007; Grosvenor et al., 2018). Limiting our analysis to low-level clouds (top < 4 km) and grid-box cloud-fractions greater than 20% for a more consistent comparison with observations, we find higher concentrations of cloud droplets in UPCAM compared to SPCAM (Fig. 1). Whereas UPCAM mitigates SPCAMs too clean conditions over much of the open ocean, particularly over the Southern Pacific Ocean, it tends to overestimate N_d over anthropogenic sources and over the Atlantic Ocean. SPCAM shows a slightly better RMSE with respect to satellite retrievals (219 cm^{-3}) compared to UPCAM (230 cm^{-3}). The similarity in skill is surprising, because UPCAM was not tuned to match observations. In terms of model differences, the higher N_{d} in UPCAM can be attributed to two aspects: a higher ratio of cloud condensation nuclei (CCN) activating into cloud droplets and a higher background CCN in the present-day (not shown). The latter is likely connected to the precipitation rate and frequency, which is a strong control of the wet scavenging of aerosols (Wood et al., 2012).

In addition to the activation of cloud condensation nuclei (CCN) into cloud droplets, the strength of the aerosol-cloud interaction also depends on the amount of baseline cloud water, for without clouds, there will be no ACI. If we plot the modeled cloud liquid water path in UPCAM and SPCAM alongside observational estimates (Elsaesser et al., 2017), we find that UPCAM shows better agreement with satellite microwave estimates, particularly in the subtropical/midlatitude regions (20° - 50°), where UPCAMs LWP bias of -25 g m^{-2} is two-thirds of SPCAMs -38 g m^{-2} bias. While the maps in Fig. 1 are based on only one year of simulation, they indicate that — even without retuning the model physics parameters to achieve a more realistic climate in the simulation (e.g., Hourdin et al., 2017) — this meteorologically nudged configuration of UPCAM that includes 2-moment microphysics produces a credible representation of clouds and aerosol-cloud processes, comparable to that in the well-documented SPCAM (Wang, Ghan, Ovchinnikov, et al., 2011; Wang et al., 2012). This gives us confidence to perform experiments simulating the cloud response to present-day anthropogenic emissions of aerosols. These UPCAM results represent an improvement from those in Parishani et al. (2017). We suspect that the use of interactive aerosols and two-moment microphysics have led to the improvement in cloud water through their tighter coupling of cloud-scale turbulence and convection with cloud microphysical processes, though nudging the meteorology might have also played a role (see Appendix A for more details.)

Now that we have established that UPCAM produces clouds realistic enough to warrant study, especially in the midlatitudes, we investigate how the cloud properties differ between simulations with present-day and pre-industrial aerosol emissions. The only difference between the present-day and pre-industrial simulations are the emissions of aerosols and aerosol precursors, namely SO2, black carbon, semi-volatile organic gas-phase species, oxidants, SO4, and organic carbon. Sea salt and dust emissions remain a function of the environmental conditions.

3.2 Quantifying the impact of anthropogenic aerosols on cloud properties

Because the winds in all UPCAM and SPCAM simulations are nudged to the same ECMWF reanalysis winds, the cloud changes due to aerosol perturbations do not feed back onto the large-scale circulation. As a result, the cloud responses in these simulations do not include any responses arising from aerosol-induced changes in the circulation, and we can study cloud responses to aerosol that — because they are independent of changes in large-scale meteorology — are as close to a pure aerosol-induced cloud re-

sponse as can be achieved in a GCM. To quantify the impact of aerosols on cloud radiative properties, we use the approximate partial radiative perturbation (APRP) method employed by Zelinka et al. (2014) to calculate Effective Radiative Forcing from aerosol-cloud interactions (ERF_{aci}) between the present-day (PD) and pre-industrial (PI) emission simulations across model configurations (Figure 2, left panels).

We begin with a cross-check on our simulation design by comparing with past work that investigated the effect of classical superparameterization on ERF_{aci}. For this comparison, we perform the same type of nudged hindcasts using version 5.1 of the conventionally parameterized Community Atmosphere Model (CAM5) to demonstrate whether the idealizations of our simulation strategy nonetheless produce consistent results with previous studies that were not as throughput-limited. Figure 2 supports this expectation, showing differences between SPCAM and CAM5 that previous studies have noted with longer simulations (Wang, Ghan, Ovchinnikov, et al., 2011; Kooperman et al., 2012): a larger increase in aerosol concentrations between present-day and pre-industrial simulations, a weaker relative increase in cloud liquid water path (LWP), and a subsequently weaker cloud radiative response (less negative) in SPCAM compared to CAM5. That we are able to reproduce previously reported results with a year of overlapped six-week nudged simulations gives us confidence that this simulation strategy captures the key differences in aerosol-cloud interactions seen across model configurations run for longer periods.

We now turn to our main interest comparing UPCAM, as the first global climate model to avoid parameterization of the boundary layer in such tests, with SPCAM and CAM5 simulations. Our focus is on the cloud response over the Northern Hemisphere (NH) midlatitude oceans north of 20°N, for three reasons. First, ERF_{aci} in this region is already known to be sensitive to how convection is parameterized (Wang, Ghan, Ovchinnikov, et al., 2011, and our Fig. 2 d,g). Second, this is where the largest increases in oceanic CCN occur relative to pre-industrial emissions scenarios (Fig. 2). Third, UPCAMs baseline marine cloud properties are least biased in this region; that is, by excluding the Tropics, we intentionally avoid most of the deep convective regions where we expect UPCAM to be less realistic (Parishani et al., 2017).

Qualitatively, compared to its precursor models, UPCAM leads to a weaker and more geographically diffuse ERF_{aci} over NH midlatitude oceans. In SPCAM and CAM5, the strongest ERF_{aci} over the NH ocean occurs over the northern stretch of the North Pacific (Fig. 2 d,g), where the LWP increase is notably high in both models (Fig. 2 f,i) with comparably little Atlantic signal. In UPCAM, the ERF_{aci} in the Pacific region is weaker (Fig. 2a), consistent with the much smaller increase in LWP in the area (Fig. 2c). Unlike the other two models, UPCAM exhibits a weak ERF_{aci} over a broader area encompassing both the North Pacific and North Atlantic.

Quantitatively, while the overall time-mean NH midlatitude ERF_{aci} of UPCAM is remarkably similar in magnitude to that of SPCAM, fundamental differences in the underlying seasonality point to distinct physics when boundary layer eddies are quasi-resolved. When we take the spatial average of ERF_{aci} over the NH ocean (Fig. 3), the annual mean shortwave ERF_{aci} in UPCAM (-2.0 W m^{-2}) is only slightly lower than in SPCAM (-2.3 W m^{-2}) (-4.0 W m^{-2} in CAM5). To see whether the ERF_{aci} differences are similar across seasons, we take the monthly mean cloud response over the NH oceans and plot the ERF_{aci} as a function of calendar month in Fig. 3. A distinct summer peak in the shortwave response occurs in SPCAM and CAM5, which mainly follows the change in insolation over the Northern Hemisphere. The UPCAM simulation, on the other hand, has its peak in ERF_{aci} in the months surrounding February. We investigate the reasons for the difference between the UPCAM and SPCAM simulations in the next section.

3.3 The $\mathbf{ERF_{aci}}$ differences between UPCAM and SPCAM

Almost all of the difference in shortwave $\mathrm{ERF_{aci}}$ is due to changes in the shortwave scattering and absorption of clouds, rather than changes in cloud cover (Fig. 3). Both an increase in N_d and an increase in cloud LWP can contribute to a brightening of the cloud and a negative $\mathrm{ERF_{aci}}$. To estimate their relative importance in explaining the model differences between SPCAM and UPCAM, we predict the change in SW radiation ΔR_{sw} as the sum of the contribution from relative N_d changes $\Delta N_\mathrm{d}/N_\mathrm{d}$ and relative liquid water path (L) changes $\Delta L/L$ building on the relationship from (Ackerman et al., 2000) (see also Bellouin et al., 2020),

$$\Delta R_{sw} = R_{sw,srf,cs,PD}\alpha_{cld,PI}(1-\alpha_{cld,PI})f_{low,PI}\left(\frac{\Delta N_\mathrm{d}}{3N_{\mathrm{d},PI}} + \frac{5\Delta L}{6L_{PI}}\right), \quad (1)$$

where $R_{sw,srf,cs,PD}$ is the surface shortwave radiation in clear-sky conditions, $\alpha_{cld,PI}$ is the pre-industrial cloud albedo, and $f_{low,PI}$ is the pre-industrial low-cloud fraction. We readily admit that the prediction based on Eq. 1 is imperfect, given that it assumes that the clouds are adiabatic, only accounts for radiative changes in low clouds, and tends to underestimate the actual change in $\mathrm{ERF_{aci}}$ (Fig. 4). Nonetheless, its physical underpinnings and the fact that it explains up to 80% of the actual $\mathrm{ERF_{aci}}$, including the seasonality differences between SPCAM and UPCAM, justifies its use in understanding them.

The solid vertical bars in Fig. 4 are the Eq. 1-predicted shortwave cloud radiative response from changes in LWP, whereas the hatched bars are those predicted from changes in N_d. Figure 4 first shows that the stronger summertime (JJA) shortwave $\mathrm{ERF_{aci}}$ in SPCAM, compared to UPCAM, can be mostly traced to a much weaker LWP response in UPCAM (Fig. 4). The $\mathrm{ERF_{aci}}$ difference between SPCAM and UPCAM is largest in the summer months when the North Pacific regions of large LWP changes in SPCAM are illuminated. The relative change of LWP in SPCAM varies little with the month of the season, but because most of the LWP response is confined to the North Pacific (Fig. 2d), its radiative impact is strongest during the boreal summer.

On the other hand, most of the stronger $\mathrm{ERF_{aci}}$ in UPCAM during the winter and fall months come from the contributions related to Nd changes. One might first suspect that this is due to a difference in the activation of cloud droplets, but actually, this difference is mainly due to UPCAM having more low clouds (Fig. 5). Because UPCAM simulates more low clouds during the winter months, particularly over the better illuminated low latitudes, the radiative impact of cloud brightening from increased cloud droplets is larger in UPCAM than in SPCAM. The differences in cloud cover, however, do not explain why SPCAM has a larger LWP contribution in Fig. 4. In the following section, we dig deeper into why the LWP response is stronger in SPCAM.

3.4 The mechanisms behind the N_d and LWP response in UPCAM and SPCAM

To better understand the conditions that lead to a larger increase in LWP in SPCAM than in UPCAM, we can match cloud conditions at a particular time and location from the present-day simulation with those from the same time and location in the pre-industrial simulation. Because the winds in pre-industrial and present-day simulations are nudged to the same ECMWF reanalysis winds, we can assume that the large-scale conditions are largely identical between the simulations. This allows us to ask the question whether a cloud that is raining in the pre-industrial simulation will respond differently to increases in aerosols compared to a cloud that is not raining (with other meteorological factors kept constant).

By distinguishing the responses of raining clouds from non-raining ones, the causes for a stronger or weaker cloud lifetime effect can be disentangled. The cloud lifetime ef-

fect, as originally described by Albrecht (1989), proposes that the LWP of an otherwise raining cloud will increase due to aerosol-induced suppression of precipitation. This presumes that the cloud would otherwise rain in the unperturbed (clean) case. In other words, we do not expect the cloud lifetime effect to impact non-raining clouds, and at least expect a smaller increase in LWP in non-raining clouds.

We separate the cloud scenes in UPCAM and SPCAM based on whether the clouds are raining in the pre-industrial simulation and examine how the liquid water path changes between the pre-industrial and present-day simulations. The difference in LWP between the present-day simulation and pre-industrial simulation (ΔL_{all}) is estimated using the response of raining cloud (ΔL_{rain}), response of non-raining clouds ($\Delta L_{non-rain}$), and the fraction of raining clouds (f):

$$\Delta L_{all} = f\Delta L_{rain} + (1-f)\Delta L_{non-rain}. \tag{2}$$

Even in simulations where winds are nudged to the same large-scale meteorology, the noisy nature of the clouds makes estimating ΔL_{rain} and $\Delta L_{non-rain}$ difficult, and some approximations and adjustments are required and are described in Appendix B. As a result, slight differences exist between estimates of ΔL_{all} (solid circles in Fig. 6) and the actual spatially averaged change in LWP (open circles in Fig. 6), but the decomposition is adequate for us to understand the differences between SPCAM and UPCAM.

Reassuringly, we find that in both UPCAM and SPCAM, the LWP response to aerosol loading is smaller in magnitude for non-raining clouds than in raining clouds, as we would expect. Comparing the UPCAM and SPCAM LWP response, we first find the LWP response in UPCAM is less than in SPCAM for most of the year. In the following, we attempt to more fully understand why UPCAM has a muted LWP response to aerosol compared to SPCAM (blue vs. orange circles) for a large part of the year. Our first finding is that although the average cloud response is lower in UPCAM, the raining cloud response in UPCAM is actually dramatically larger than in SPCAM. In other words, hiding behind the first-order impression of a muted LWP response to aerosol loading is a stronger sensitivity of LWP to increasing aerosol in raining cloud in UPCAM than in SPCAM. Thus the reason the overall LWP response is weaker in UPCAM must be linked to the other two factors: the response of non-raining clouds and the baseline fraction of raining clouds (or the probability of precipitation). Large-eddy simulations (Ackerman et al., 2004; Bretherton et al., 2007; Chen et al., 2011) and some observations (Chen et al., 2014; Toll et al., 2017) report the existence of both positive and negative responses of LWP to aerosols, where LWP tends to decrease with increasing aerosols in thin, non-raining clouds. These findings lend support for the overall weak and slightly negative LWP response of non-raining clouds in UPCAM.

If we shift our focus to the baseline fraction of raining clouds in low-lying clouds, we can see from Fig. 7 that the fraction of precipitating clouds as a function of LWP is indeed lower in UPCAM than in SPCAM. Climate models, in general, show a tendency to overpredict the probability of precipitation (POP – Stephens et al., 2010), and even in SPCAM (Kooperman et al., 2016). Furthermore, Mlmenstdt et al. (2020) point out the importance of establishing the baseline precipitation frequency to better constrain the aerosol-cloud interactions. L'Ecuyer et al. (2009) provide such an estimate of POP based on CloudSat, and a comparison of Fig. 6 of this study with Fig. 1 of L'Ecuyer et al. (2009) suggests that the precipitation fraction in UPCAM is more consistent with the POP from L'Ecuyer et al. (2009). However, differences in averaging length and area of study between L'Ecuyer et al. (2009) and this study make it difficult to conclude strongly which is more realistic.

In summary, the analysis presented in this section and further elaborated in Appendix B provides evidence that the lower increase in LWP with aerosols in UPCAM is

due to a weaker LWP increase in non-raining clouds and a small fraction of raining clouds in the baseline climate.

4 Discussion and conclusions

We now discuss three implications of our findings. First, the results support the idea that a targeted analysis of aerosol-cloud interactions that differentiates the response of raining and non-raining clouds can help us gain a better conceptual understanding of why two different models produce different aerosol-cloud interactions. The simulation strategy of nudging large-scale winds inhibits feedbacks of aerosols on circulation but allows a unique test-bed for studying aerosol-cloud interaction. Based on previous global studies (e.g., Wang et al., 2012), we approached the analysis expecting the response of raining clouds to aerosol perturbations to be the largest differentiator of aerosol-cloud interaction between the models. However, when we separate our analysis into clouds that rain and do not rain, we find that other factors, namely the baseline fraction of clouds that rain and the response of non-raining clouds, better explain the overall difference in LWP response to aerosols in UPCAM compared to SPCAM. This distinction of ACI in raining and non-raining clouds has been done in previous observational analyses (e.g., Possner et al., 2020; Toll et al., 2017), but here we show how an analogous distinction of ACI in raining versus non-raining clouds can be done even in global models, and proves helpful in understanding emergent ACI effects, provided we nudge the large-scale conditions.

One might then ask, whether SPCAM or UPCAM more realistically capture those factors that we identify as major contributors differentiating the UPCAM from the SPCAM cloud response. LES simulations support a weakly positive or negative response of LWP to increases in aeorsols in non-precipitating clouds, and CloudSat retrievals of the baseline fraction of raining clouds (or probability of precipitation; L'Ecuyer et al., 2009) appear to better match UPCAM's baseline fraction. However, there are many caveats to the comparison with observations, including the difference in horizontal averaging length, which is important to make a consistent assessment of probability of precipitation. The study of L'Ecuyer et al. (2009) also encompasses a larger region over the oceans, compared to the focus of northern hemisphere midlatitude clouds in this study. Mlmenstdt et al. (2020) further report the potential importance of differentiating between drizzle and rain to better constrain model behavior. Exploring these are beyond the scope of this study, but highlight observational estimates that will be important for better assessing aerosol cloud interactions in models.

We also find that the LWP response of non-raining clouds in UPCAM is negative, while it is positive in SPCAM. Large-eddy simulations of idealized low-level clouds exhibit a decrease in LWP for non-raining clouds (Ackerman et al., 2004; Chen et al., 2011), supporting the UPCAM response, but going forward, what will be important is to observationally quantify the extent to which the LWP decreases with aerosol and to identify how and whether the response differs as a function of meteorology and season.

Other metrics, such as precipitation susceptibility, also have been identified to better connect individual processes with the overall LWP response to aerosols, where the advantages of the susceptibility metric is that it can be estimated using observations (Sorooshian et al., 2009; Terai et al., 2012; Wang et al., 2012; Mann et al., 2014). Here, we view the simulation strategy and analysis in this study as a complementary approach that helps us better confront our cartoon model of the aerosol-cloud interactions.

A second implication of our study is that the seasonal cycle in the aerosol cloud interactions can differ between different model configurations (SPCAM and UPCAM). This result highlights the importance of covering a wide range of meteorological contexts and seasons when comparing aerosol-cloud interactions particularly in high resolution

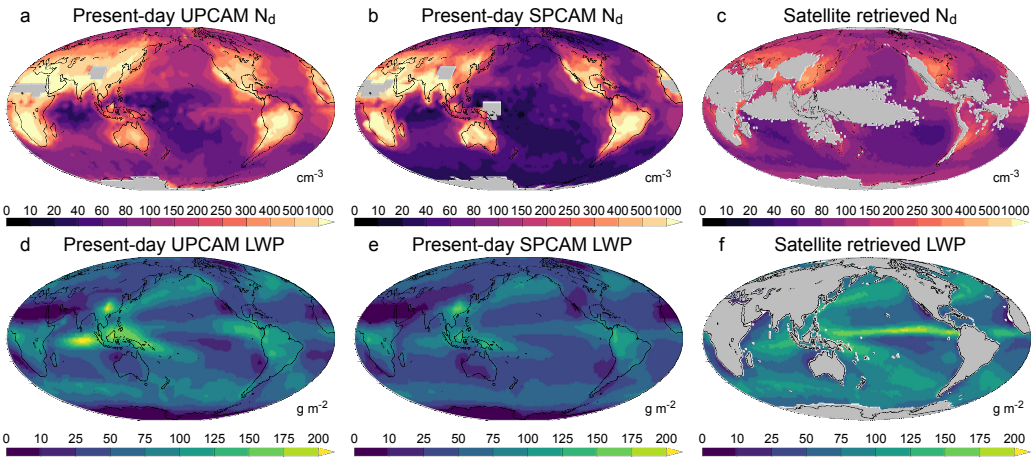

Figure 1. (top row) The cloud top cloud droplet number concentration (Nd, cm^{-3}) in UPCAM (a) and SPCAM (b) and a passive satellite retrieval based estimate of cloud droplet number concentration from Grosvenor et al., (2018) (c). (bottom row) The cloud liquid water path (LWP; g m^{-2}) in UPCAM (d), in SPCAM (e), and from microwave retrievals of Elsaesser et al. (2017) (f).

models where computational costs of running simulations constrains decisions about the variety and duration of simulations.

Third and perhaps most importantly, this study reinforces the need for comparison of aerosol-cloud interactions in limited-area high resolution simulations (LES) with global simulations. This study reveals that by resolving the scales of boundary layer eddies, we arrive at a conceptually different picture of the aerosol-cloud interaction than one might get from looking at a model that resolves up to the km-scale motions. Even as we move towards storm- or cloud-resolving global simulations (e.g., Sato et al., 2018; Stevens et al., 2019), we are still some years off from resolving the boundary layer eddies in global models (Bellouin et al., 2020). There are subgrid turbulence parameterizations that can bridge those sub-kilometer unresolved scales (Larson et al., 2012; Bogenschutz & Krueger, 2013; Xu & Cheng, 2016; K. Zhang et al., 2017), but their impact on ACI remains to be seen. Therefore, as increased computational capacities allow for larger domains and longer simulations using large-eddy models, this study stresses the importance of consistently comparing aerosol-cloud interaction between global and local-scale simulations to gain perspective on areas that need improvement in global models and which will ultimately yield a more reliable global estimate of the radiative impact of aerosol-cloud interaction.

Appendix A Difference in one-moment versus two-moment UPCAM

This study differs from the UPCAM simulations in Parishani et al. (2018) in a number of ways. Whereas the simulations in Parishani et al. (2018) were free-running, used single moment microphysics, prescribed aerosol concentrations, and were run at $2^\circ \times 2^\circ$ horizontal resolution in the GCM, the simulations in this study had winds nudged every 6-hours, used two-moment microphysics, used the MAM3 prognostic aerosol scheme coupled to cloud-resolving eddy statistics with the Explicit Convection Parameterized Pollution scheme, and were run at $4^\circ \times 5^\circ$ horizontal resolution in the GCM. In addi-

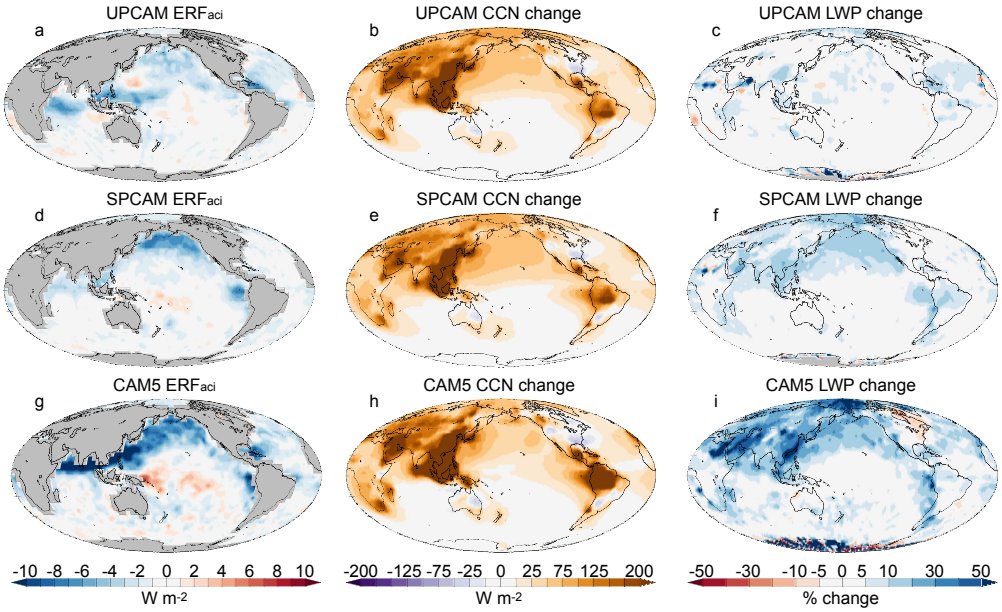

Figure 2. The effective radiative forcing from aerosol-cloud interactions (ERF_{aci}; left column), percent change in CCN concentration (middle column), and percent change in cloud liquid water path (right column) in UPCAM (top row), SPCAM (middle row), and CAM5 (bottom row).

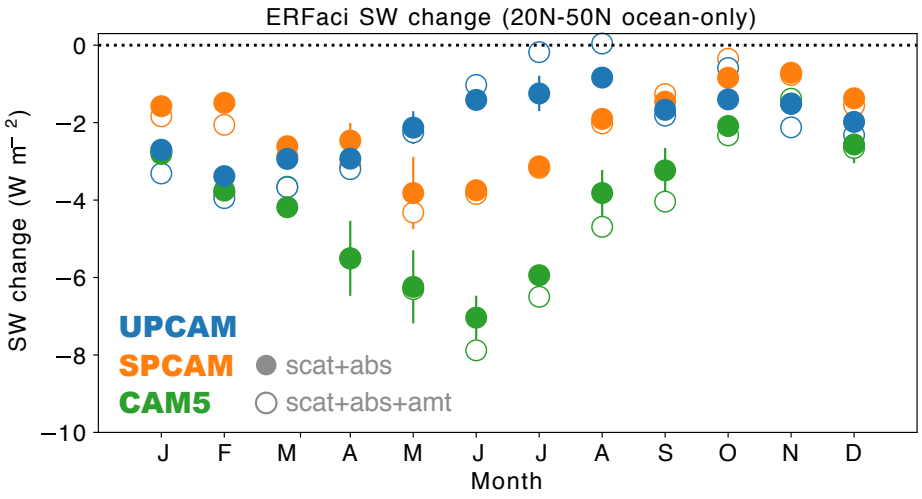

Figure 3. The ERF_{aci} from scattering and absorption averaged over the Northern Hemisphere ocean (20°N−50°N) in UPCAM (blue), SPCAM (orange), and CAM5 (green). Vertical lines indicate the 95% confidence interval of the mean taken from daily variations over the four-week averaging period. Despite agreeing on the time-mean, UPCAM and SPCAM have distinct seasonal cycles of ERF_{aci}.

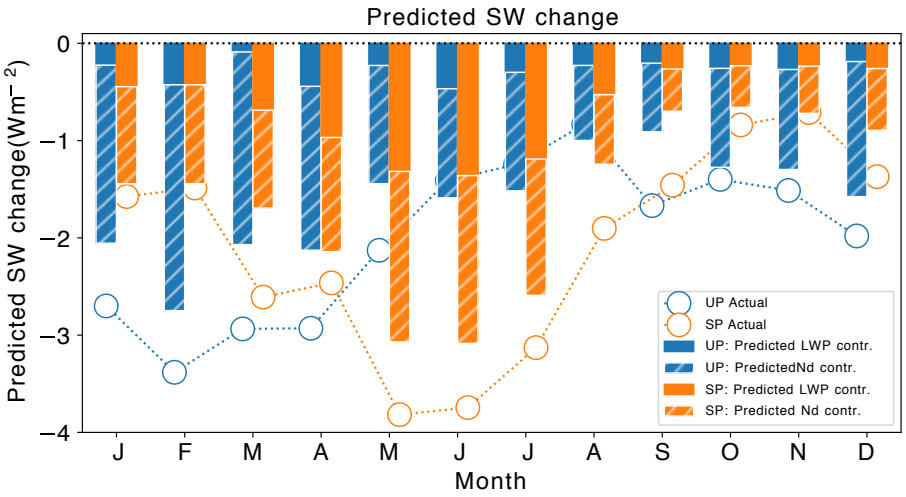

Figure 4. Parameterized decomposition of the model seasonal cycle differences, i.e. ΔR_{sw} of Eq. 1 predicted for UPCAM (blue) and SPCAM (orange) as a function of calendar months. The total $\overline{\Delta R_{sw}}$ is separated into contributions from LWP changes (solid color) and from N_d changes (hatching). Open circles in the background indicate the change in SW cloud radiation estimated using the APRP method of Zelinka et al. (2014) in which analogous inter-model seasonality differences justify the parameterization.

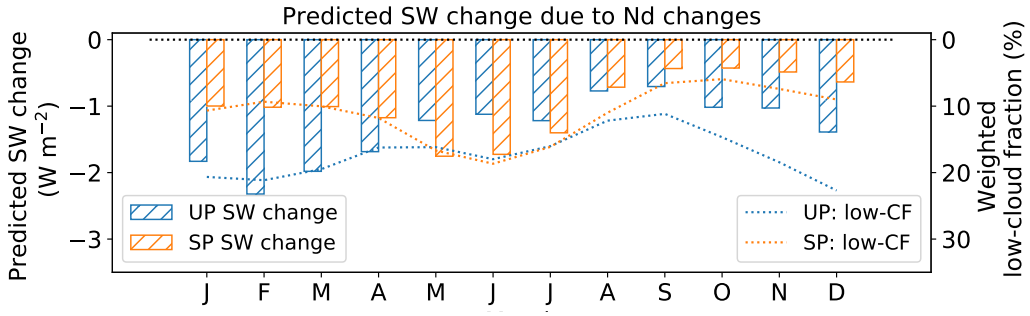

Figure 5. The predicted SW change over the NH ocean due to relative N_d changes in UPCAM (blue) and SPCAM (orange) are shown as hatched bars. Dotted lines indicate the low-cloud fractions, weighted by insolation (see right y-axis for scale).

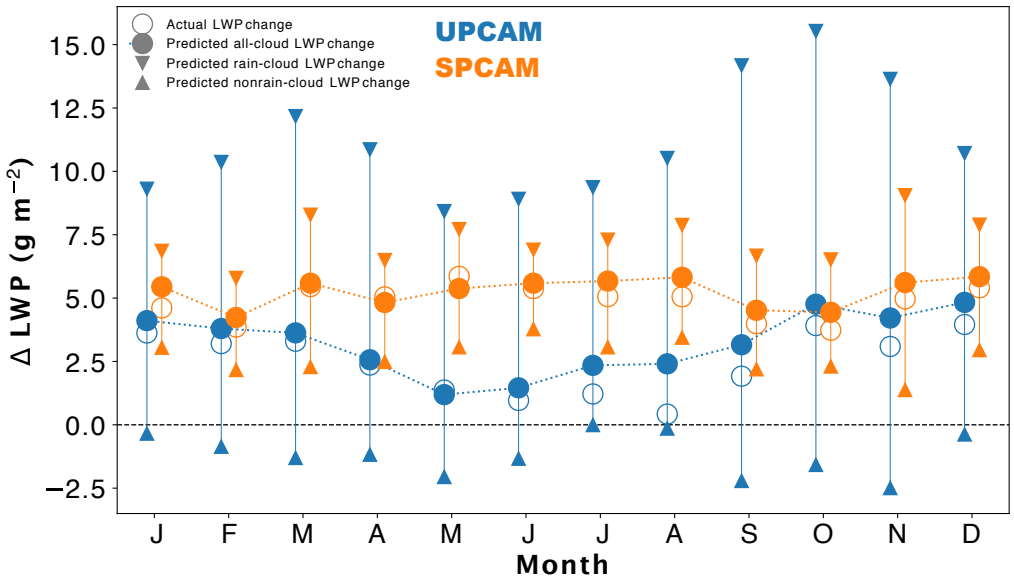

Figure 6. Northern Hemisphere (20°N−50°N) LWP difference over oceans (filled circles) between pre-industrial and present-day simulations as a function of calendar month in UPCAM (blue) and SPCAM (orange). Predictions are based on a decomposition after raining (down-pointed triangles) and non-raining cloud LWP responses (up-pointed triangles) are separated and their responses are scaled by the fraction of raining and non-raining clouds as in Eq. 2. Open circles indicate actual differences in the LWP between present-day and pre-industrial simulations over the same area.

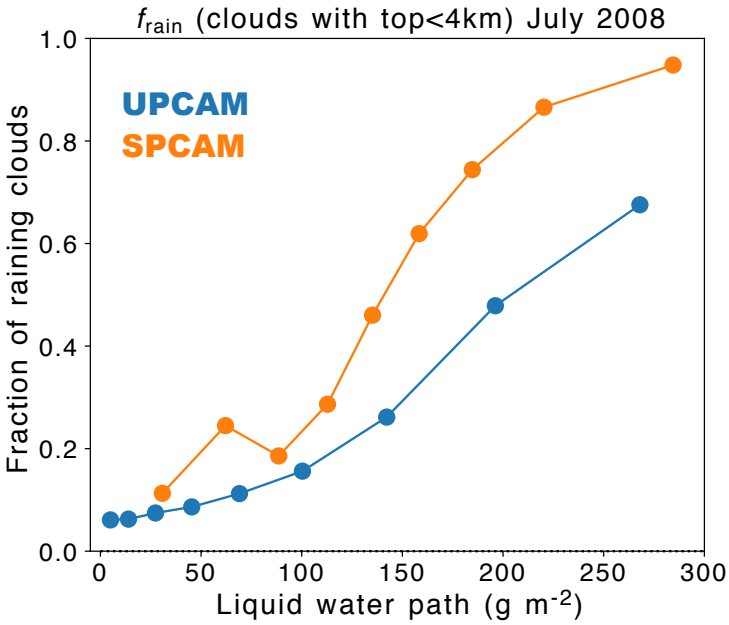

Figure 7. Probability of precipitation (using a threshold of 0.6 mm/d) as a function of cloudy-scene liquid water path over Northern Hemisphere (20°N−50°N) oceans in the month of July. Blue indicates UPCAM and orange indicates SPCAM.

Table A1. Global mean top-of-atmosphere radiative fluxes and cloud properties in UP-AER (of this study), UPCAM of Parishani et al. (2018), and from observational estimates (CERES EBAF v4.1 for radiative fluxes and Elsaesser et al. (2017) for LWP.)

Model	TOA SW ($W\ m^{-2}$)	TOA LW ($W\ m^{-2}$)	LWP ($g\ m^{-2}$)	Low cloud fraction (%) (%)
UP-AER (this study)	227	218	59.0 [67.3*]	37
UPCAM (P18^{+})	245	240	54.3	48
Satellite obs	241	240	82.1*	N/A

$^{+}$ Parishani et al. (2018). * Mean LWP averaged only over ocean.

tion, because of its large computational cost and especially slow throughput, this model was not tuned in any fashion so that the top-of-atmosphere model matched observations.

Despite this difference, it is still instructive to examine the large-scale climate diagnostics of the model. Table A1 below notes the top of atmosphere net shortwave flux (TOA SW) and net longwave flux (TOA LW), the global mean liquid water path (LWP), and the global mean low-cloud fraction. Despite having a smaller coverage of low clouds, the prognostic aerosol version of UPCAM (UP-AER) in this study has more cloud reflection and a larger LWP. For reference, the TOA SW radiation is compared with CERES EBAF v4.1 climatological mean in Fig. A1. We find that UP-AER, despite not being tuned and still showing too much absorbed shortwave, improves on the larger solar absorption bias over the stratocumulus region reported in Parishani et al. (2018) and also has fairly small biases over most of the midlatitude oceans. However, the deep convective clouds over the tropical west Pacific are too reflective, leading to a large negative bias in top-of-atmosphere shortwave radiation in UP-AER. The same deep convective regions are also the main source for the negative bias in outgoing TOA LW radiation.

Appendix B Separating out the aerosol-mediated cloud response in raining and non-raining clouds

In this section we explain how we calculate the aerosol-cloud adjustment in raining and non-raining clouds. We first separate snapshots of cloudy GCM grid columns in the pre-industrial simulation based on whether or not they are raining using a rain threshold of 0.6 mm d^{-1}. Since meteorology is nudged identically, each snapshot in the pre-industrial simulation has a corresponding snapshot in the present-day simulation, where the geographic location, time of day, and large-scale meteorology match with those of the pre-industrial simulation.

We might naively then take the cloud response to aerosol perturbations to be equal to the difference in the liquid water path between the present-day and pre-industrial snapshot. However, that difference does not take into account a level of stochasticity (randomness) inherent in all clouds, including superparameterized clouds (Jones et al., 2019).

Because of this stochasticity, even if were to examine two simulations with the same aerosol emission scenarios and meteorological nudging, there will be some LWP cloud difference in each snapshot comparison. For example, if the LWP is anomalously higher in the first simulation it will tend towards the mean in the second simulation and produce a negative change in LWP. Now when we separate the clouds into those that are raining and those that are not, we end up selecting clouds with higher anomalous cloud LWP. Therefore, if we were then to look at the LWP change in two simulations with the

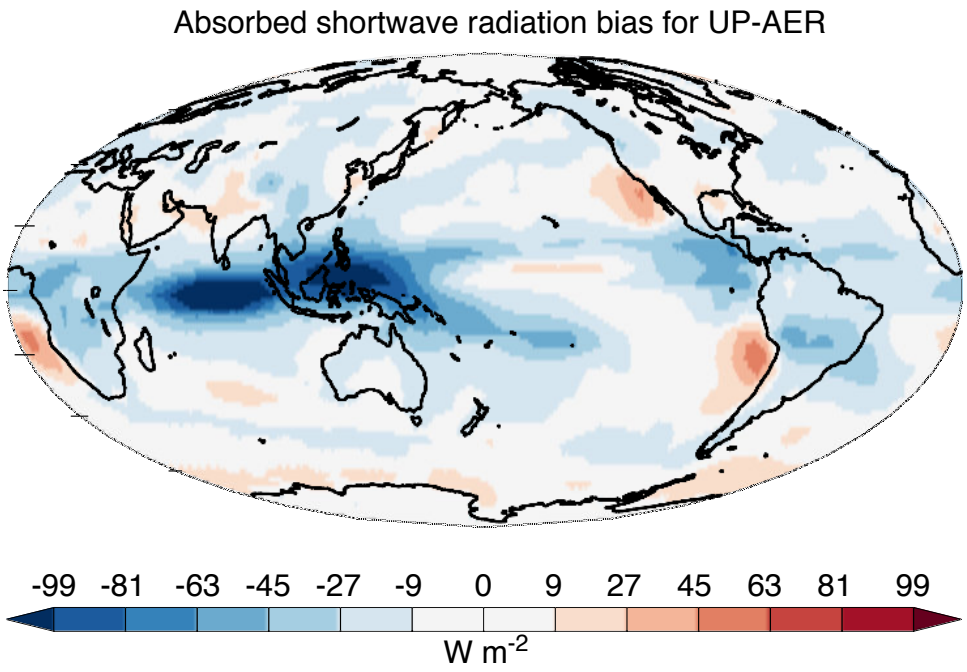

Figure A1. Difference in top-of-atmosphere absorbed shortwave radiation between UP-AER and CERES-EBAF v4.1. Units in W m−2.

same LWP distribution, we would find that the change in LWP of raining clouds is negative, while the change of non-raining clouds is positive. Note that this negative response of raining clouds is purely due to the stochasticity of clouds and does not have any physical mechanism behind it.

The extent to with which we will see this effect is a function of both the difference in mean LWP of raining and non-raining clouds but also a function of the correlation between the LWP in the first and second simulation. If the LWP in the first simulation perfectly matches the LWP in the second simulation, then we would not see this effect. On the other hand, if it happened that the geographic location, time of day, and large-scale meteorology has no impact on LWP, we would see zero correlation in the LWP of the first and second simulation and this regression to the mean effect will be strongest.

To take into account the impact of stochasticity on our analysis, we therefore apply a correction term that is a function of both the LWP anomaly for a snapshot x ($L_{(x,PI)} - \overline{L_{x,PI}}$) and the correlation between the snapshots from the present-day and pre-industrial simulations ($r(L_{PI}, L_{PD})$). Therefore, the corrected LWP change (ΔL_x) is formulated as

$$\Delta L_x = L_{x,PD} - (L_{x,PI} - \overline{L_{all,PI}})[1 - r(L_{PI}, L_{PD})] \tag{B1}$$

In this way, the correction factor $(L_{(x,PI)} - \overline{L_{x,PI}})[1 - r(L_{PI}, L_{PD})]$ will go to zero as the stochasticity goes to zero and $(r(L_{PI}, L_{PD}))$ goes to one. An advantage of this correction is that when all instances are aggregated, they sum to zero. Using this corrected LWP response for each snapshot, we aggregate all the raining and non-raining cloud instances from the pre-industrial simulation to produce a total monthly-mean ΔL_{all} as a function of the mean raining cloud response ΔL_{rain} and mean non-raining cloud response $\Delta L_{non-rain}$ as in Eq. 2.

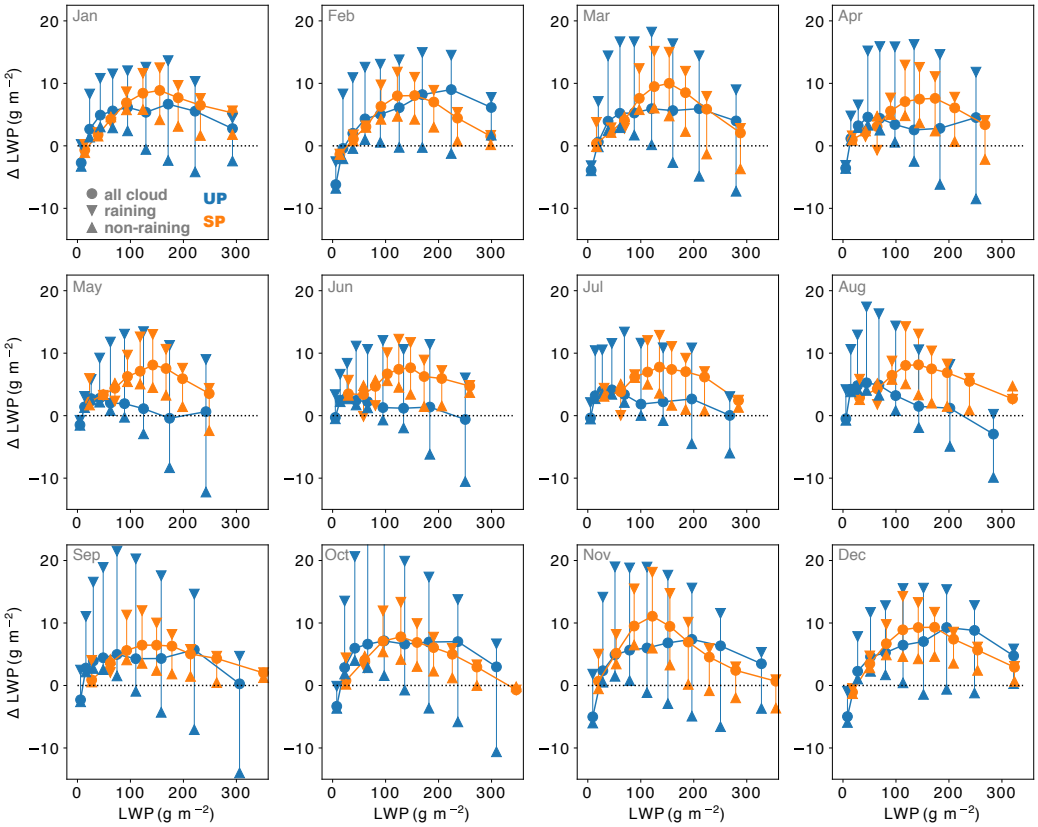

Figure B1. The difference in liquid water path (solid lines) between present-day and pre-industrial simulations as a function of pre-industrial LWP in UPCAM (blue) and SPCAM (orange). Dashed lines indicate the LWP differences in pre-industrial raining scenes, while dotted lines indicate LWP differences in non-raining scenes. All twelve calendar months are shown.

Figure B1 shows how ΔL_{all}, ΔL_{rain}, and $\Delta L_{non-rain}$ vary as a function of LWP in UPCAM and SPCAM. Matching expectation from our conceptual understanding, we find that the LWP response in raining clouds is more positive than the response in non-raining clouds in both SPCAM and UPCAM across all months and they peak in intermediate values of LWP. Matching the monthly-means in Fig. 6, we also find that ΔL_{rain} in UPCAM tends to lie above ΔL_{rain} in SPCAM, which indicates that the raining cloud response is not the reason for the lower overall LWP response in UPCAM. Instead, it is UPCAM's lower $\Delta L_{non-rain}$ and smaller f.

Acknowledgments

The work was supported by the U.S. Department of Energy's Exascale Computing Project (17-SC-20-SC) and by the National Science Foundation's Climate and Large-Scale Dynamics Program (AGS-1912134). Part of CRT's contribution was conducted under the auspices of the U.S. Department of Energy by Lawrence Livermore National Laboratory under Contract DE-AC52-07NA27344.

This research also used HPC resources of the Extreme Science and Engineering Discovery Environment (XSEDE), which is supported by National Science Foundation grant number ACI-1548562 (Towns et al., 2014) and allocation number TG-ATM190002, and of the National Energy Research Scientific Computing Center (NERSC), which is a U.S.

Department of Energy Office of Science User Facility operated under Contract DE-AC02-05CH11231. IM Release: LLNL-JRNL-812724-DRAFT

The daily cloud droplet number concentration retrievals cited in this study and in Grosvenor et al. (2018) can be retrieved at the following site (`https://catalogue.ceda.ac.uk/uuid/cf97ccc802d348ec8a3b6f2995dfbbff`). The satellite LWP retrievals of this study can be accessed through the Goddard Earth Sciences Data and Information Services Center (`https://disc.gsfc.nasa.gov/datasets/MACLWP_mean_1/summary?keywords=MAC%20LWP`). Finally, the CERES EBAF v4.1 satellite data can be retrieved from NASA's Atmospheric Science Data Center (`https://eosweb.larc.nasa.gov/project/ceres/ebaf_ed4.1`). Processed model output relevant for this data can be found here: `https://zenodo.org/record/3968813#.XySdtvhKg0o`.

We acknowledge and thank contributions from Hossein Parishani for the initial development of UPCAM as well as feedback on early stages of the work.

References

Ackerman, A. S., Kirkpatrick, M. P., Stevens, D. E., & Toon, O. B. (2004, December). The impact of humidity above stratiform clouds on indirect aerosol climate forcing. *Nature*, *432*(7020), 1014–1017. doi: 10.1038/nature03174

Ackerman, A. S., Toon, O. B., Taylor, J. P., Johnson, D. W., Hobbs, P. V., & Ferek, R. J. (2000, August). Effects of Aerosols on Cloud Albedo: Evaluation of Twomeys Parameterization of Cloud Susceptibility Using Measurements of Ship Tracks. *Journal of the Atmospheric Sciences*, *57*(16), 2684–2695. doi: 10.1175/1520-0469(2000)057⟨2684:EOAOCA⟩2.0.CO;2

Albrecht, B. A. (1989, September). Aerosols, Cloud Microphysics, and Fractional Cloudiness. *Science*, *245*(4923), 1227–1230. doi: 10.1126/science.245.4923.1227

Bellouin, N., Quaas, J., Gryspeerdt, E., Kinne, S., Stier, P., WatsonParris, D., ... Stevens, B. (2020). Bounding Global Aerosol Radiative Forcing of Climate Change. *Reviews of Geophysics*, *58*(1), e2019RG000660. doi: 10.1029/2019RG000660

Bennartz, R. (2007). Global assessment of marine boundary layer cloud droplet number concentration from satellite. *Journal of Geophysical Research: Atmospheres*, *112*(D2). doi: 10.1029/2006JD007547

Bogenschutz, P. A., & Krueger, S. K. (2013). A simplified pdf parameterization of subgrid-scale clouds and turbulence for cloud-resolving models. *Journal of Advances in Modeling Earth Systems*, *5*(2), 195-211. doi: 10.1002/jame.20018

Bretherton, C. S., Blossey, P. N., & Uchida, J. (2007). Cloud droplet sedimentation, entrainment efficiency, and subtropical stratocumulus albedo. *Geophysical Research Letters*, *34*(3). doi: 10.1029/2006GL027648

Chen, Y.-C., Christensen, M. W., Stephens, G. L., & Seinfeld, J. H. (2014, September). Satellite-based estimate of global aerosolcloud radiative forcing by marine warm clouds. *Nature Geoscience*, *7*(9), 643–646. doi: 10.1038/ngeo2214

Chen, Y.-C., Xue, L., Lebo, Z. J., Wang, H., Rasmussen, R. M., & Seinfeld, J. H. (2011, September). A comprehensive numerical study of aerosol-cloud-precipitation interactions in marine stratocumulus. *Atmospheric Chemistry and Physics*, *11*(18), 9749–9769. doi: https://doi.org/10.5194/acp-11-9749-2011

Dee, D. P., Uppala, S. M., Simmons, A. J., Berrisford, P., Poli, P., Kobayashi, S., ... Vitart, F. (2011). The era-interim reanalysis: configuration and performance of the data assimilation system [Journal Article]. *Quarterly Journal of the Royal Meteorological Society*, *137*(656), 553-597. Retrieved from `<GotoISI>://WOS:000290450900001` doi: 10.1002/qj.828

Elsaesser, G. S., ODell, C. W., Lebsock, M. D., Bennartz, R., Greenwald, T. J., &

Wentz, F. J. (2017, December). The Multisensor Advanced Climatology of Liquid Water Path (MAC-LWP). *Journal of Climate*, *30*(24), 10193–10210. doi: 10.1175/JCLI-D-16-0902.1

Grabowski, W. W. (2001, May). Coupling Cloud Processes with the Large-Scale Dynamics Using the Cloud-Resolving Convection Parameterization (CRCP). *Journal of the Atmospheric Sciences*, *58*(9), 978–997. doi: 10.1175/1520-0469(2001)058⟨0978:CCPWTL⟩2.0.CO;2

Grosvenor, D. P., Sourdeval, O., Zuidema, P., Ackerman, A., Alexandrov, M. D., Bennartz, R., ... Quaas, J. (2018). Remote Sensing of Droplet Number Concentration in Warm Clouds: A Review of the Current State of Knowledge and Perspectives. *Reviews of Geophysics*, *56*(2), 409–453. doi: 10.1029/2017RG000593

Gustafson, W. I., Berg, L. K., Easter, R. C., & Ghan, S. J. (2008, April). The Explicit-Cloud Parameterized-Pollutant hybrid approach for aerosolcloud interactions in multiscale modeling framework models: tracer transport results. *Environmental Research Letters*, *3*(2), 025005. doi: 10.1088/1748-9326/3/2/025005

Hill, A. A., Feingold, G., & Jiang, H. (2009, May). The Influence of Entrainment and Mixing Assumption on AerosolCloud Interactions in Marine Stratocumulus. *Journal of the Atmospheric Sciences*, *66*(5), 1450–1464. doi: 10.1175/2008JAS2909.1

Hourdin, F., Mauritsen, T., Gettelman, A., Golaz, J.-C., Balaji, V., Duan, Q., ... Williamson, D. (2017, March). The Art and Science of Climate Model Tuning. *Bulletin of the American Meteorological Society*, *98*(3), 589–602. doi: 10.1175/BAMS-D-15-00135.1

Iacono, M. J., Delamere, J. S., Mlawer, E. J., Shephard, M. W., Clough, S. A., & Collins, W. D. (2008). Radiative forcing by long-lived greenhouse gases: Calculations with the AER radiative transfer models. *Journal of Geophysical Research: Atmospheres*, *113*(D13). doi: 10.1029/2008JD009944

IPCC. (2014). Clouds and aerosols. In *Climate change 2013 - the physical science basis* (pp. 571–658). Cambridge University Press. Retrieved from `http://dx.doi.org/10.1017/CBO9781107415324.016` (Cambridge Books Online)

Jing, X., & Suzuki, K. (2018). The Impact of Process-Based Warm Rain Constraints on the Aerosol Indirect Effect. *Geophysical Research Letters*, *45*(19), 10,729–10,737. doi: 10.1029/2018GL079956

Jones, T. R., Randall, D. A., & Branson, M. D. (2019). Multiple-instance superparameterization: 2. the effects of stochastic convection on the simulated climate. *Journal of Advances in Modeling Earth Systems*, *11*(11), 3521-3544. Retrieved from `https://agupubs.onlinelibrary.wiley.com/doi/abs/10.1029/2019MS001611` doi: 10.1029/2019MS001611

Khairoutdinov, M., Randall, D., & DeMott, C. (2005, July). Simulations of the Atmospheric General Circulation Using a Cloud-Resolving Model as a Superparameterization of Physical Processes. *Journal of the Atmospheric Sciences*, *62*(7), 2136–2154. doi: 10.1175/JAS3453.1

Kooperman, G. J., Pritchard, M. S., Burt, M. A., Branson, M. D., & Randall, D. A. (2016). Robust effects of cloud superparameterization on simulated daily rainfall intensity statistics across multiple versions of the Community Earth System Model. *Journal of Advances in Modeling Earth Systems*, *8*(1), 140–165. doi: 10.1002/2015MS000574

Kooperman, G. J., Pritchard, M. S., Ghan, S. J., Wang, M., Somerville, R. C. J., & Russell, L. M. (2012). Constraining the influence of natural variability to improve estimates of global aerosol indirect effects in a nudged version of the Community Atmosphere Model 5. *Journal of Geophysical Research: Atmospheres*, *117*(D23). doi: 10.1029/2012JD018588

Larson, V. E., Schanen, D. P., Wang, M., Ovchinnikov, M., & Ghan, S. (2012). PDF

669 Parameterization of Boundary Layer Clouds in Models with Horizontal Grid
670 Spacings from 2 to 16 km. *Monthly Weather Review*, *140*(1), 285-306.
671 L'Ecuyer, T. S., Berg, W., Haynes, J., Lebsock, M., & Takemura, T. (2009). Global
672 observations of aerosol impacts on precipitation occurrence in warm mar-
673 itime clouds. *Journal of Geophysical Research: Atmospheres*, *114*(D9). doi:
674 10.1029/2008JD011273
675 Liu, X., Easter, R. C., Ghan, S. J., Zaveri, R., Rasch, P., Shi, X., ... Mitchell,
676 D. (2012, May). Toward a minimal representation of aerosols in cli-
677 mate models: description and evaluation in the Community Atmosphere
678 Model CAM5. *Geoscientific Model Development*, *5*(3), 709–739. doi:
679 https://doi.org/10.5194/gmd-5-709-2012
680 Mann, J. A. L., Chiu, J. C., Hogan, R. J., O'Connor, E. J., L'Ecuyer, T. S., Stein,
681 T. H. M., & Jefferson, A. (2014). Aerosol impacts on drizzle properties in
682 warm clouds from ARM Mobile Facility maritime and continental deploy-
683 ments. *Journal of Geophysical Research: Atmospheres*, *119*(7), 4136–4148. doi:
684 10.1002/2013JD021339
685 Michibata, T., Suzuki, K., Sato, Y., & Takemura, T. (2016, December). The source
686 of discrepancies in aerosolcloudprecipitation interactions between GCM and
687 A-Train retrievals. *Atmospheric Chemistry and Physics*, *16*(23), 15413–15424.
688 doi: https://doi.org/10.5194/acp-16-15413-2016
689 Mlawer, E. J., Taubman, S. J., Brown, P. D., Iacono, M. J., & Clough, S. A. (1997).
690 Radiative transfer for inhomogeneous atmospheres: RRTM, a validated
691 correlated-k model for the longwave. *Journal of Geophysical Research: At-*
692 *mospheres*, *102*(D14), 16663–16682. doi: 10.1029/97JD00237
693 Mlmenstdt, J., Nam, C., Salzmann, M., Kretzschmar, J., LEcuyer, T. S., Lohmann,
694 U., ... Quaas, J. (2020, May). Reducing the aerosol forcing uncertainty using
695 observational constraints on warm rain processes. *Science Advances*, *6*(22),
696 eaaz6433. doi: 10.1126/sciadv.aaz6433
697 Morrison, H., & Gettelman, A. (2008, August). A New Two-Moment Bulk Strati-
698 form Cloud Microphysics Scheme in the Community Atmosphere Model, Ver-
699 sion 3 (CAM3). Part I: Description and Numerical Tests. *Journal of Climate*,
700 *21*(15), 3642–3659. doi: 10.1175/2008JCLI2105.1
701 Neale, R. B., Chen, C. C., Gettelman, A., Lauritzen, P. H., Park, S., & Williamson,
702 D. L. (2012, November). *Description of the ncar community atmosphere*
703 *model (cam 5.0)* (Tech. Rep. Nos. NCAR/TN-486 + STR). Boulder, Colorado:
704 National Center For Atmospheric Research.
705 Parishani, H., Pritchard, M. S., Bretherton, C. S., Terai, C. R., Wyant, M. C.,
706 Khairoutdinov, M., & Singh, B. (2018). Insensitivity of the Cloud Response
707 to Surface Warming Under Radical Changes to Boundary Layer Turbu-
708 lence and Cloud Microphysics: Results From the Ultraparameterized CAM.
709 *Journal of Advances in Modeling Earth Systems*, *10*(12), 3139–3158. doi:
710 10.1029/2018MS001409
711 Parishani, H., Pritchard, M. S., Bretherton, C. S., Wyant, M. C., & Khairoutdinov,
712 M. (2017). Toward low-cloud-permitting cloud superparameterization with
713 explicit boundary layer turbulence. *Journal of Advances in Modeling Earth*
714 *Systems*, *9*(3), 1542–1571. doi: 10.1002/2017MS000968
715 Park, S., & Bretherton, C. S. (2009, June). The University of Washington Shallow
716 Convection and Moist Turbulence Schemes and Their Impact on Climate Sim-
717 ulations with the Community Atmosphere Model. *Journal of Climate*, *22*(12),
718 3449–3469. doi: 10.1175/2008JCLI2557.1
719 Pincus, R., & Baker, M. B. (1994, November). Effect of precipitation on the albedo
720 susceptibility of clouds in the marine boundary layer. *Nature*, *372*(6503), 250–
721 252. doi: 10.1038/372250a0
722 Possner, A., Eastman, R., Bender, F., & Glassmeier, F. (2020, March). Deconvo-
723 lution of boundary layer depth and aerosol constraints on cloud water path in

subtropical stratocumulus decks. *Atmospheric Chemistry and Physics*, *20*(6), 3609–3621. doi: https://doi.org/10.5194/acp-20-3609-2020

Randall, D., Khairoutdinov, M., Arakawa, A., & Grabowski, W. (2003, November). Breaking the Cloud Parameterization Deadlock. *Bulletin of the American Meteorological Society*, *84*(11), 1547–1564. doi: 10.1175/BAMS-84-11-1547

Randall, D. A. (2013). Beyond deadlock. *Geophysical Research Letters*, *40*(22), 5970–5976. Retrieved 2020-06-17, from `https://agupubs.onlinelibrary.wiley.com/doi/abs/10.1002/2013GL057998` doi: 10.1002/2013GL057998

Sato, Y., Goto, D., Michibata, T., Suzuki, K., Takemura, T., Tomita, H., & Nakajima, T. (2018, March). Aerosol effects on cloud water amounts were successfully simulated by a global cloud-system resolving model. *Nature Communications*, *9*(1), 1–7. doi: 10.1038/s41467-018-03379-6

Schneider, T., Teixeira, J., Bretherton, C. S., Brient, F., Pressel, K. G., Schr, C., & Siebesma, A. P. (2017, January). Climate goals and computing the future of clouds. *Nature Climate Change*, *7*(1), 3–5. doi: 10.1038/nclimate3190

Sorooshian, A., Feingold, G., Lebsock, M. D., Jiang, H., & Stephens, G. L. (2009, July). On the precipitation susceptibility of clouds to aerosol perturbations. *Geophysical Research Letters*, *36*(13), L13803. doi: 10.1029/2009GL038993

Stephens, G. L., L'Ecuyer, T., Forbes, R., Gettlemen, A., Golaz, J.-C., Bodas-Salcedo, A., ... Haynes, J. (2010). Dreary state of precipitation in global models [Journal Article]. *Journal of Geophysical Research-Atmospheres*, *115*. doi: 10.1029/2010jd014532

Stevens, B., Satoh, M., Auger, L., Biercamp, J., Bretherton, C. S., Chen, X., ... Zhou, L. (2019, September). DYAMOND: the DYnamics of the Atmospheric general circulation Modeled On Non-hydrostatic Domains. *Progress in Earth and Planetary Science*, *6*(1), 61. Retrieved from `https://doi.org/10.1186/s40645-019-0304-z` doi: 10.1186/s40645-019-0304-z

Suzuki, K., Golaz, J.-C., & Stephens, G. L. (2013). Evaluating cloud tuning in a climate model with satellite observations. *Geophysical Research Letters*, *40*(16), 4464–4468. doi: 10.1002/grl.50874

Terai, C. R., Wood, R., Leon, D. C., & Zuidema, P. (2012, May). Does precipitation susceptibility vary with increasing cloud thickness in marine stratocumulus? *Atmospheric Chemistry and Physics*, *12*(10), 4567–4583. doi: 10.5194/acp-12-4567-2012

Toll, V., Christensen, M., Gass, S., & Bellouin, N. (2017). Volcano and Ship Tracks Indicate Excessive Aerosol-Induced Cloud Water Increases in a Climate Model. *Geophysical Research Letters*, *44*(24), 12,492–12,500. doi: 10.1002/2017GL075280

Towns, J., Cockerill, T., Dahan, M., Foster, I., Gaither, K., Grimshaw, A., ... Wilkins-Diehr, N. (2014, September). XSEDE: Accelerating Scientific Discovery. *Computing in Science Engineering*, *16*(5), 62–74. doi: 10.1109/MCSE.2014.80

Twomey, S. (1977, July). The Influence of Pollution on the Shortwave Albedo of Clouds. *Journal of the Atmospheric Sciences*, *34*(7), 1149–1152. doi: 10.1175/1520-0469(1977)034⟨1149:TIOPOT⟩2.0.CO;2

Wang, M., Ghan, S., Easter, R., Ovchinnikov, M., Liu, X., Kassianov, E., ... Morrison, H. (2011, March). The multi-scale aerosol-climate model PNNL-MMF: model description and evaluation. *Geoscientific Model Development*, *4*(1), 137–168. doi: https://doi.org/10.5194/gmd-4-137-2011

Wang, M., Ghan, S., Liu, X., L'Ecuyer, T. S., Zhang, K., Morrison, H., ... Penner, J. E. (2012). Constraining cloud lifetime effects of aerosols using A-Train satellite observations. *Geophysical Research Letters*, *39*(15). doi: 10.1029/2012GL052204

Wang, M., Ghan, S., Ovchinnikov, M., Liu, X., Easter, R., Kassianov, E., ... Morrison, H. (2011, June). Aerosol indirect effects in a multi-scale aerosol-climate

model PNNL-MMF. *Atmospheric Chemistry and Physics*, *11*(11), 5431–5455. doi: https://doi.org/10.5194/acp-11-5431-2011

Wood, R., Leon, D., Lebsock, M., Snider, J., & Clarke, A. D. (2012). Precipitation driving of droplet concentration variability in marine low clouds. *Journal of Geophysical Research: Atmospheres*, *117*(D19). doi: 10.1029/2012JD018305

Xu, K.-M., & Cheng, A. (2016). Understanding the tropical cloud feedback from an analysis of the circulation and stability regimes simulated from an upgraded multiscale modeling framework. *Journal of Advances in Modeling Earth Systems*, *8*(4), 1825-1846. doi: 10.1002/2016MS000767

Zelinka, M. D., Andrews, T., Forster, P. M., & Taylor, K. E. (2014). Quantifying components of aerosol-cloud-radiation interactions in climate models. *Journal of Geophysical Research: Atmospheres*, *119*(12), 7599–7615. doi: 10.1002/2014JD021710

Zhang, G. J., & McFarlane, N. A. (1995, September). Sensitivity of climate simulations to the parameterization of cumulus convection in the Canadian climate centre general circulation model. *Atmosphere-Ocean*, *33*(3), 407–446. doi: 10.1080/07055900.1995.9649539

Zhang, K., Fu, R., Shaikh, M. J., Ghan, S., Wang, M., Leung, L. R., ... Marengo, J. (2017). Influence of Superparameterization and a Higher-Order Turbulence Closure on Rainfall Bias Over Amazonia in Community Atmosphere Model Version 5. *Journal of Geophysical Research: Atmospheres*, *122*(18), 9879–9902. doi: 10.1002/2017JD026576

Zhang, K., Wan, H., Liu, X., Ghan, S. J., Kooperman, G. J., Ma, P.-L., ... Lohmann, U. (2014, August). Technical Note: On the use of nudging for aerosolclimate model intercomparison studies. *Atmospheric Chemistry and Physics*, *14*(16), 8631–8645. doi: https://doi.org/10.5194/acp-14-8631-2014

Zhang, S., Wang, M., Ghan, S. J., Ding, A., Wang, H., Zhang, K., ... Fu, C. (2016, March). On the characteristics of aerosol indirect effect based on dynamic regimes in global climate models. *Atmospheric Chemistry and Physics*, *16*(5), 2765–2783. doi: https://doi.org/10.5194/acp-16-2765-2016

Figure 1.

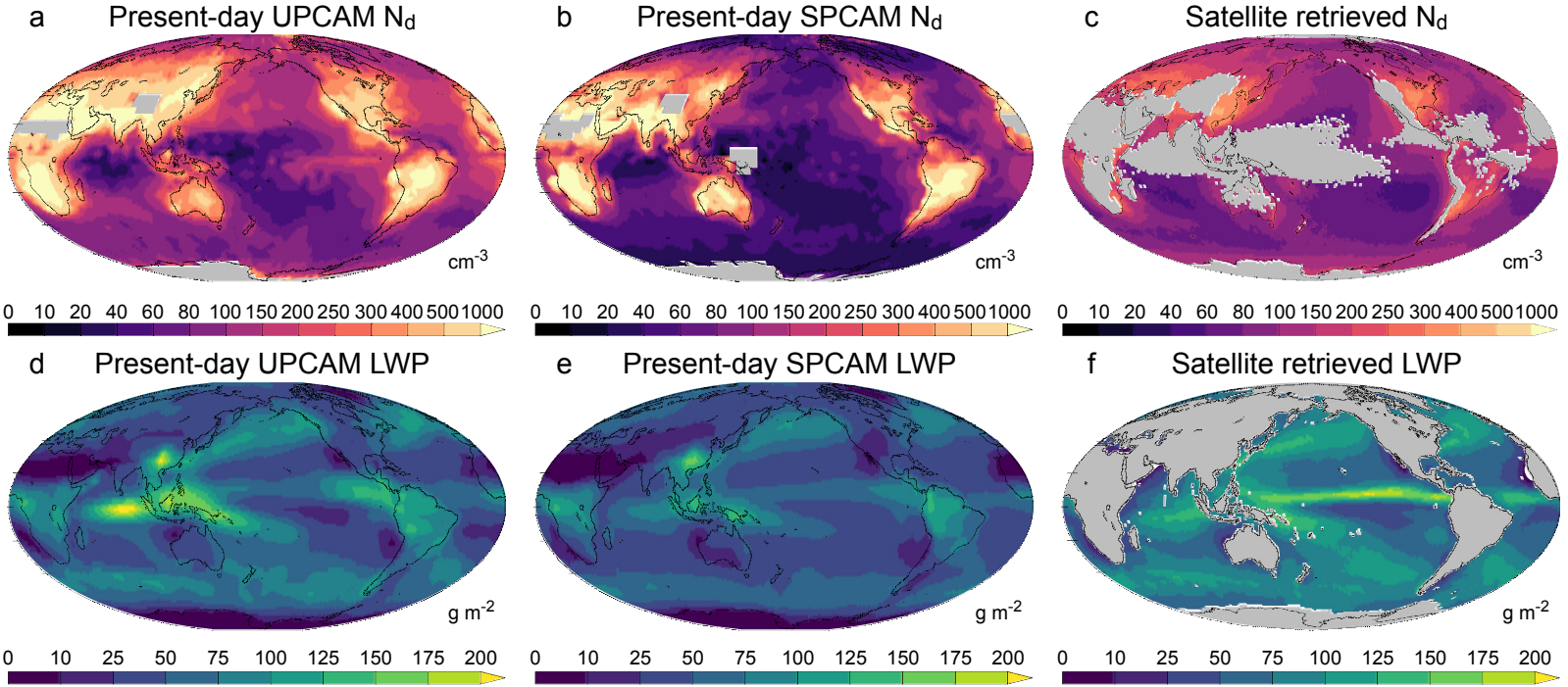
a
Present-day UPCAM N_d
b
Present-day SPCAM N_d
c
Satellite retrieved N_d
cm^{-3}
0 10 20 40 60 80 100 150 200 250 300 400 500 1000
d
Present-day UPCAM LWP
e
Present-day SPCAM LWP
f
Satellite retrieved LWP
g m^{-2}
0 10 25 50 75 100 125 150 175 200

Figure 2.

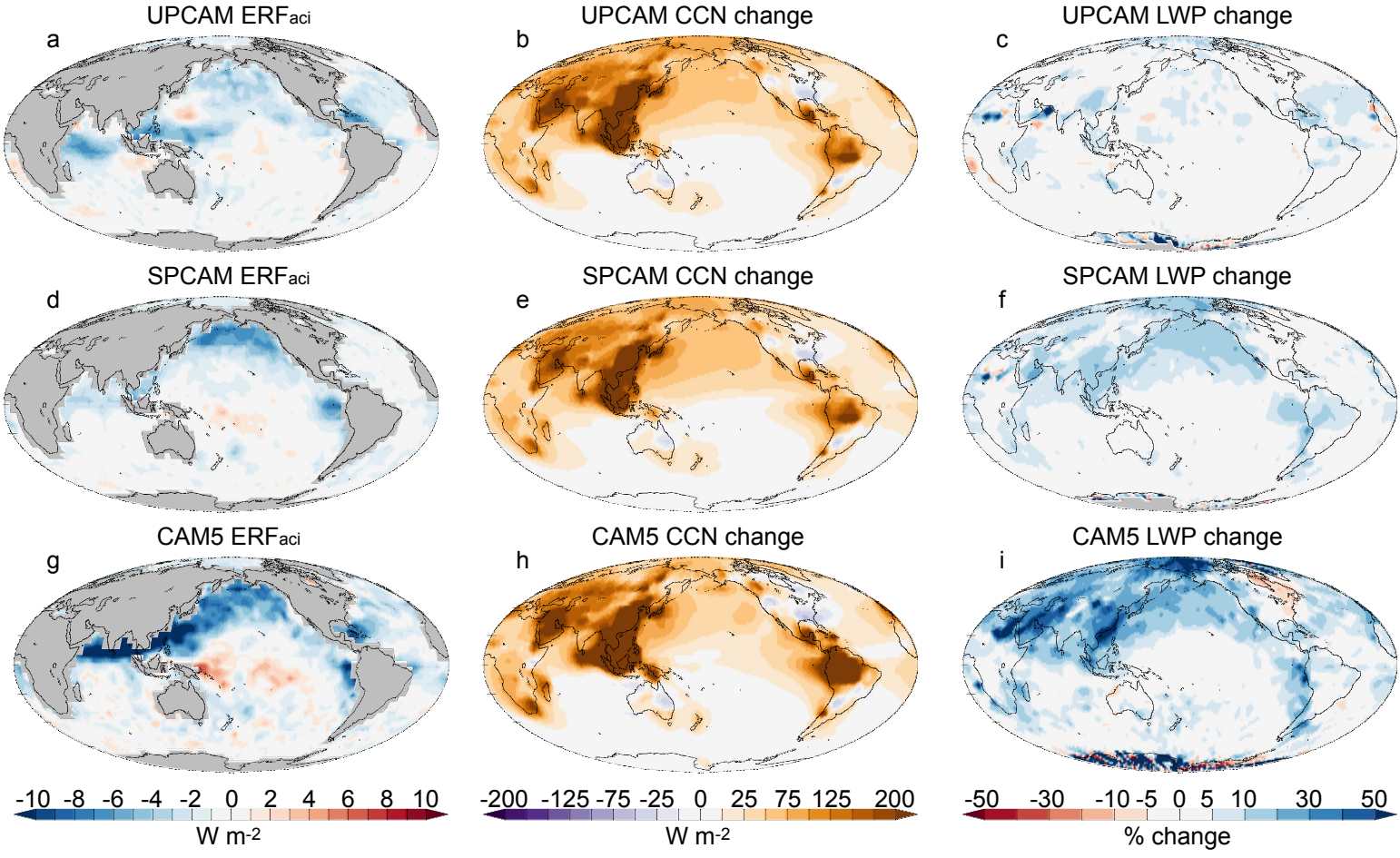
UPCAM ERFaci
a
UPCAM CCN change
b
UPCAM LWP change
c
SPCAM ERFaci
d
SPCAM CCN change
e
SPCAM LWP change
f
CAM5 ERFaci
g
CAM5 CCN change
h
CAM5 LWP change
i
-10 -8 -6 -4 -2 0 2 4 6 8 10
W m-2
-200 -125 -75 -25 0 25 75 125 200
W m-2
-50 -30 -10 -5 0 5 10 30 50
% change

Figure 3.

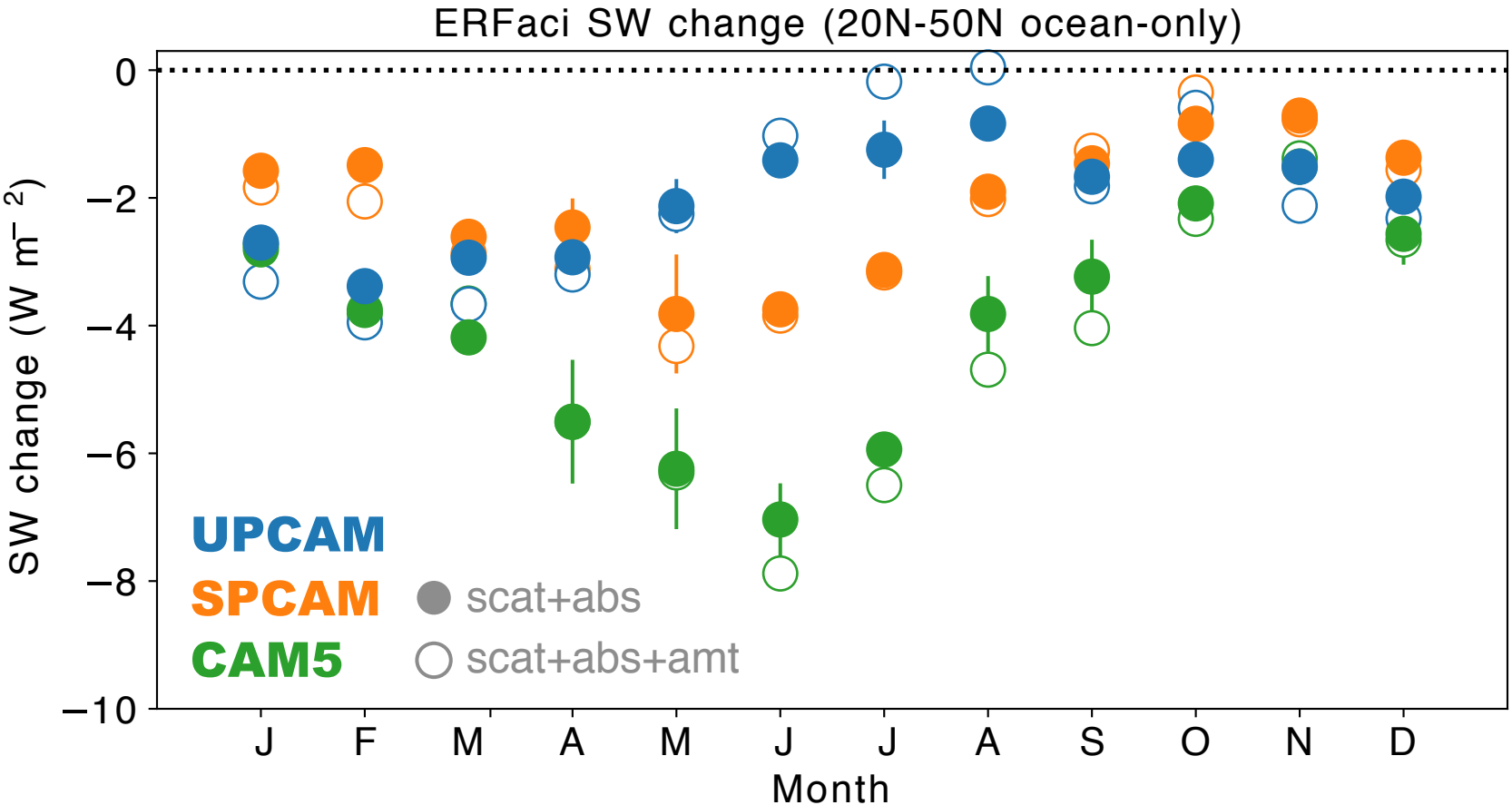
ERFaci SW change (20N-50N ocean-only)
SW change (W m⁻²)
0
−2
−4
−6
−8
−10
J
F
M
A
M
J
J
A
S
O
N
D
Month
UPCAM
SPCAM
CAM5
scat+abs
scat+abs+amt

Figure 4.

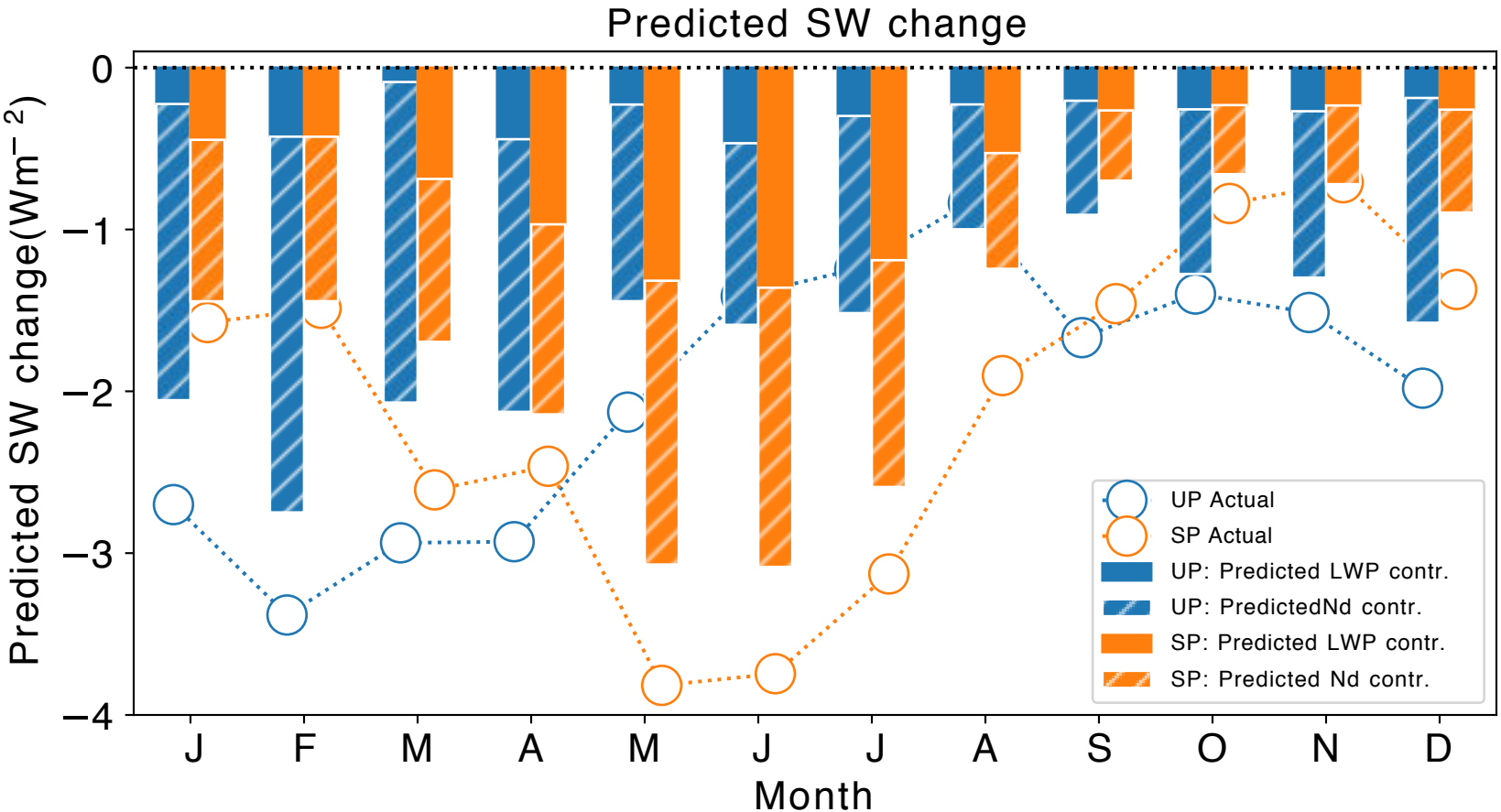
Predicted SW change
Predicted SW change(Wm^{-2})
0
−1
−2
−3
−4
J
F
M
A
M
J
J
A
S
O
N
D
Month
UP Actual
SP Actual
UP: Predicted LWP contr.
UP: PredictedNd contr.
SP: Predicted LWP contr.
SP: Predicted Nd contr.

Figure 5.

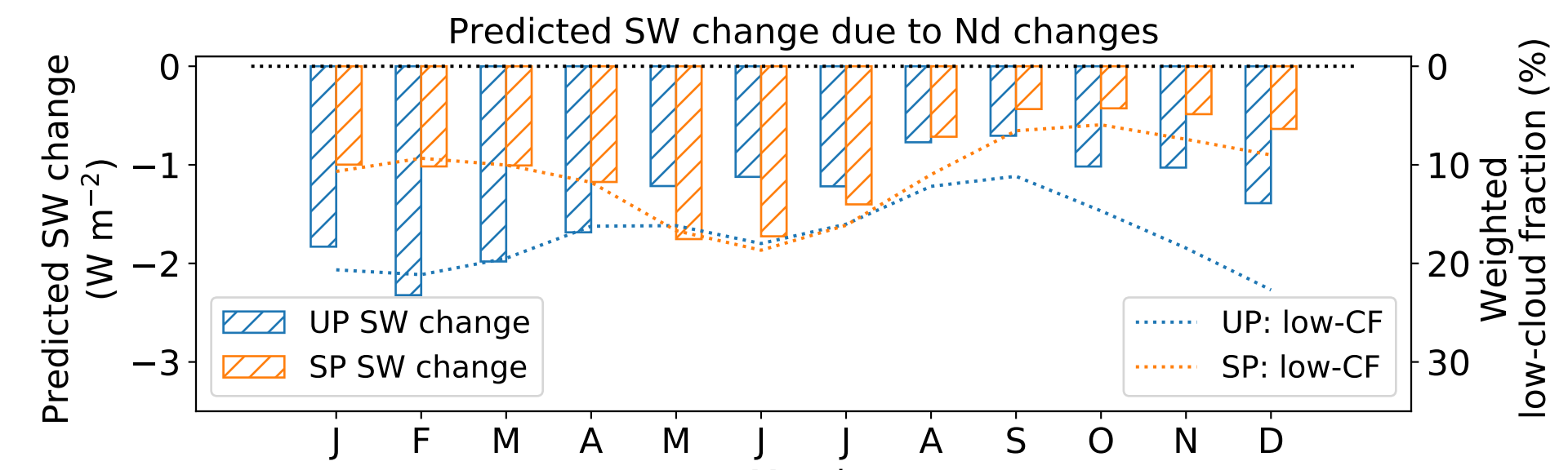
Predicted SW change due to Nd changes
Predicted SW change (W m^{-2})
0
−1
−2
−3
Weighted low-cloud fraction (%)
0
10
20
30
UP SW change
SP SW change
UP: low-CF
SP: low-CF
J
F
M
A
M
J
J
A
S
O
N
D

Figure 6.

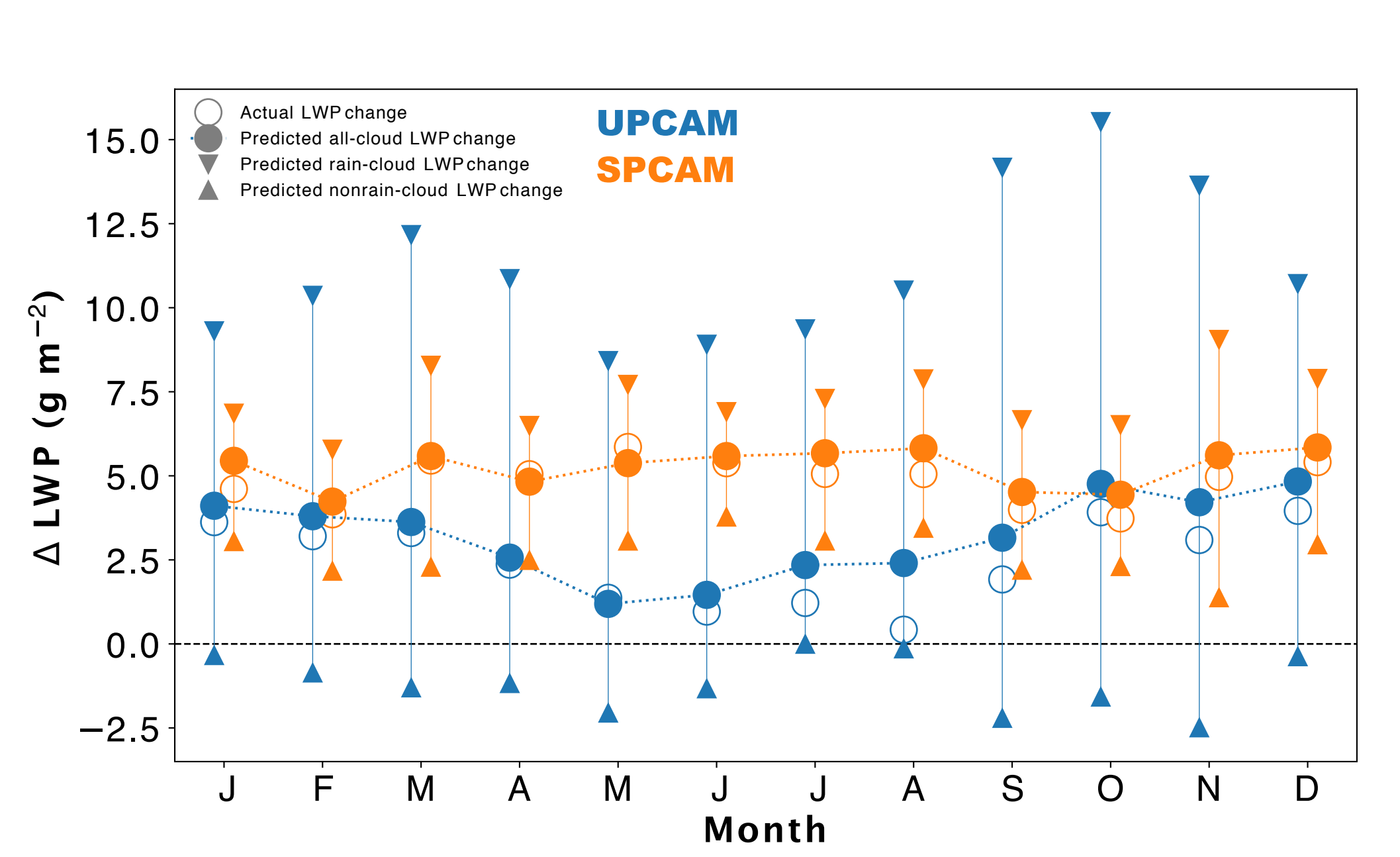
Actual LWP change
Predicted all-cloud LWP change
Predicted rain-cloud LWP change
Predicted nonrain-cloud LWP change
UPCAM
SPCAM
15.0
12.5
10.0
7.5
5.0
2.5
0.0
−2.5
Δ LWP (g m−2)
J
F
M
A
M
J
J
A
S
O
N
D
Month

Figure 7.

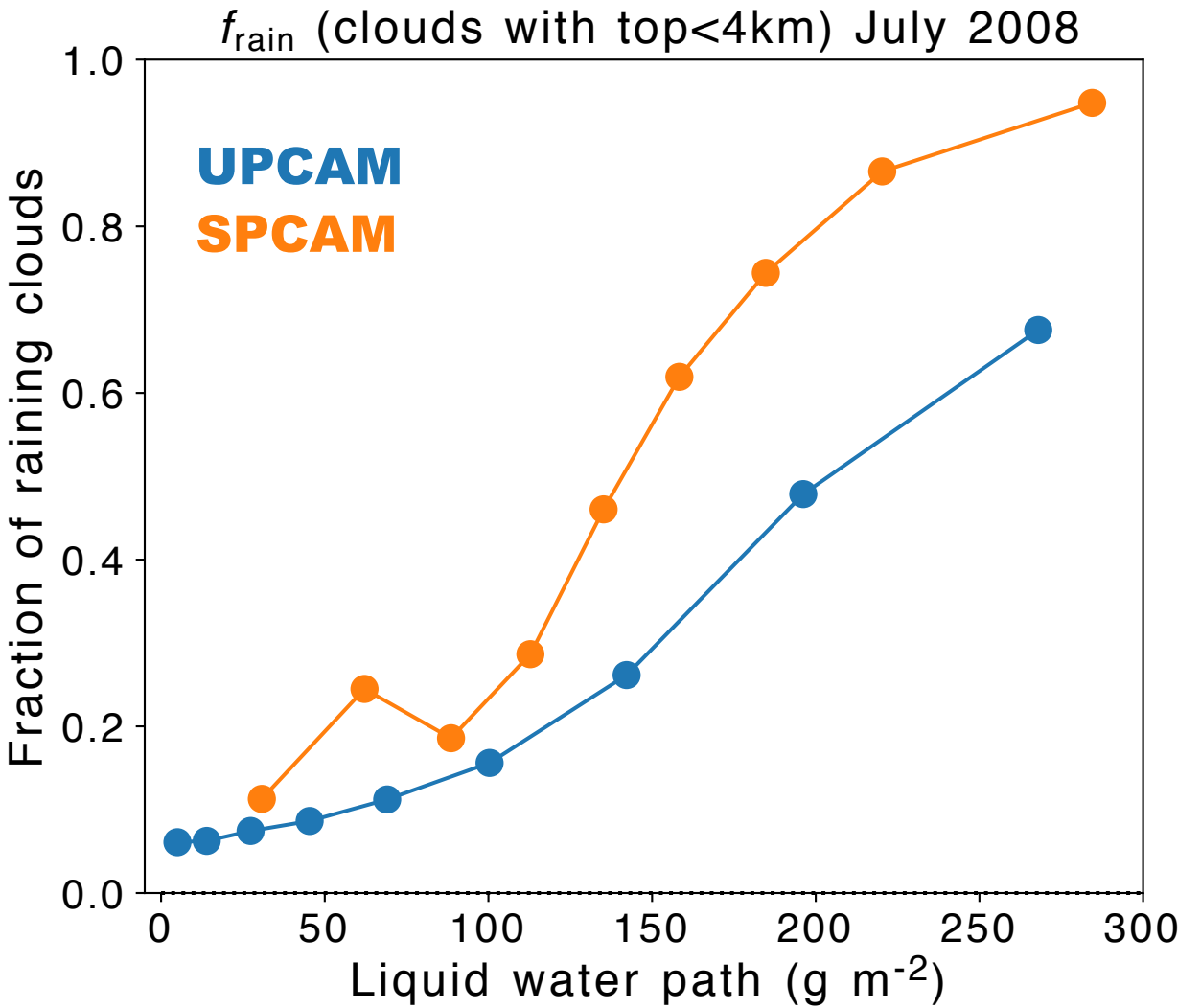
f_{rain} (clouds with top<4km) July 2008
UPCAM
SPCAM
Fraction of raining clouds
1.0
0.8
0.6
0.4
0.2
0.0
0
50
100
150
200
250
300
Liquid water path (g m^{-2})

Figure A1.

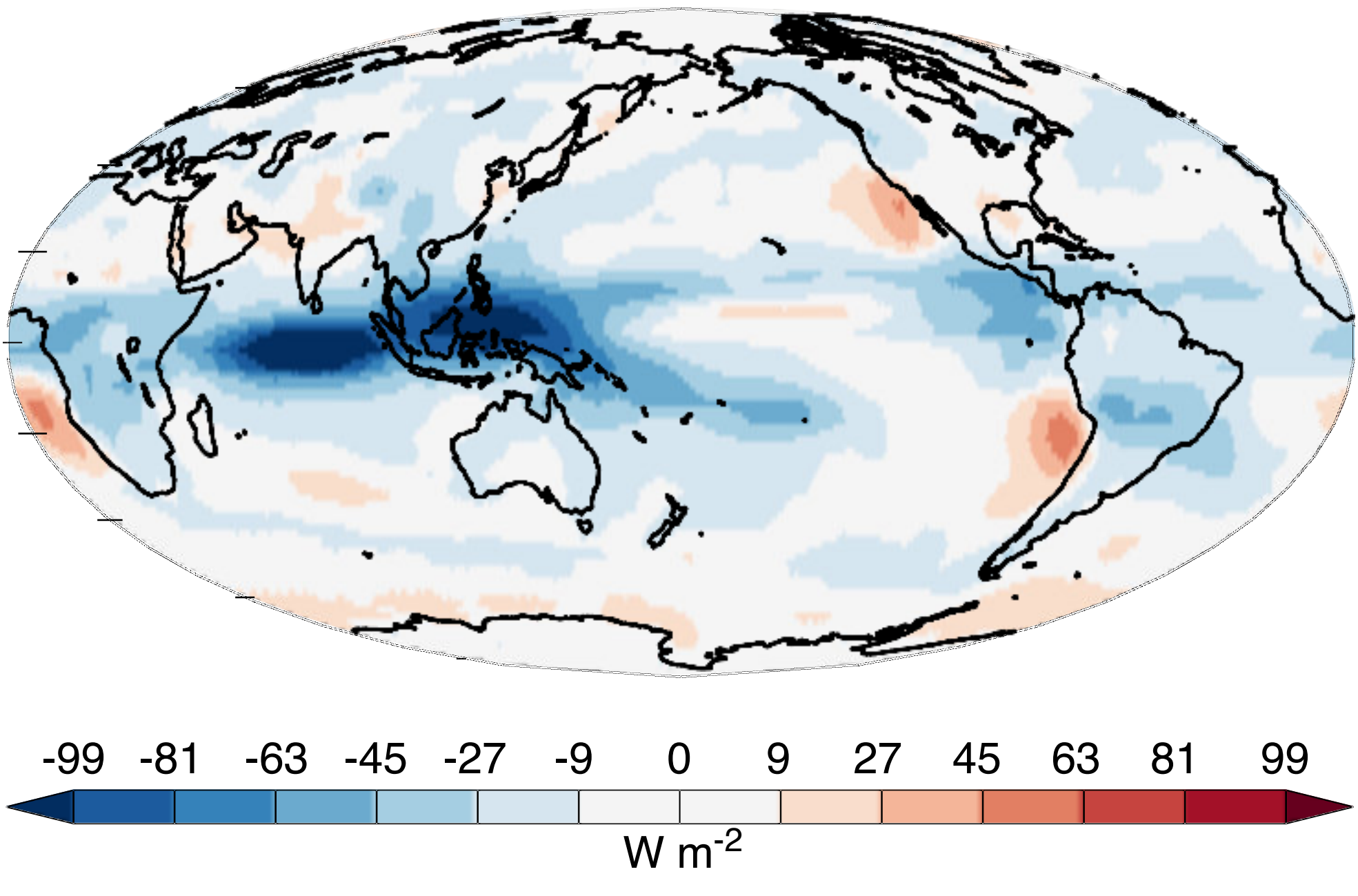
Absorbed shortwave radiation bias for UP-AER
-99 -81 -63 -45 -27 -9 0 9 27 45 63 81 99
W m-2

Figure B1.

Jan
Feb
Mar
Apr
May
Jun
Jul
Aug
Sep
Oct
Nov
Dec
all cloud
raining
non-raining
UP
SP
Δ LWP (g m^{-2})
LWP (g m^{-2})
20
10
0
−10
0
100
200
300